



Color from invisible flicker: a failure of the Talbot–Plateau law caused by an early ‘hard’ saturating nonlinearity used to partition the human short-wave cone pathway

Andrew Stockman ^{a,*}, Daniel J. Plummer ^b

^a *Department of Psychology, University of California San Diego, 9500 Gilman Drive, La Jolla, CA 92093-0109, USA*

^b *Department of Ophthalmology, Shiley Eye Center, University of California San Diego School of Medicine, La Jolla, CA 92093-0946, USA*

Received 18 June 1997; received in revised form 29 December 1997

Abstract

The Talbot–Plateau law fails for flicker detected by the short-wavelength-sensitive (S) cones: a 30–40 Hz target, flickering too fast for the flicker to be resolved, looks more yellow than a steady target of the same average intensity. The color change, which is produced by distortion at an early compressive nonlinearity, was used to reveal a slightly bandpass S-cone temporal response before the distortion site and a lowpass response after it. The nonlinearity is probably a ‘hard’ nonlinearity that arises because the S-cone signal is limited by a response ceiling, which the mean signal level approaches and exceeds as the S-cone adaptation level increases. The nonlinearity precedes the combination of flicker signals from all three cone types. © 1998 Elsevier Science Ltd. All rights reserved.

Keywords: Color; S-cones; Nonlinearity; Flicker; Talbot–Plateau law; Temporal

1. Introduction

It is well known that flickering a light, while keeping its average intensity constant, can alter its appearance. Indeed, there are bodies of literature both on the changes in brightness [1–6] and on the changes in color [7–10] that are caused by flicker. Such changes are the result of nonlinearities in the visual system.

An important generalization about the visual effects of flicker was made by Talbot [11] and Plateau [12], who noted that the flicker must be visible for it to alter the appearance of a flickering light. Thus, lights flickering at rates above the temporal resolution limit (i.e. above the critical flicker frequency or CFF), above which flicker is invisible, should appear identical to steady lights of the same average intensity and chromaticity. Given the ample evidence that the early stages of the visual system can follow flicker at rates well above the observer’s CFF [13,14], this generalization is

important because it implies that—at least for flicker above the CFF—the early visual stages must be operating in an approximately linear range. If they were not, nonlinear distortion would alter the appearance of the invisibly flickering lights, and the Talbot–Plateau law would fail.

Fig. 1 shows a simplified linear model of a visual system that obeys the Talbot–Plateau law. The top panel shows two cycles of the input signal (the visual stimulus). The second panel summarizes the early stages of the visual system as an early linear temporal filter, which produces the intermediate signal shown in the middle panel. The intermediate signal depends on the early filter, which will scale and delay the frequency components in the input signal (in this case, three components, as described in the next paragraph) according to its transmission characteristics. The penultimate panel represents a late temporal filter that transmits low frequency flicker but selectively attenuates high frequency flicker. Lastly, the bottom panel shows two cycles of the output signal, which in this case is a constant. We assume that the output signal is the basis of the subjects’ responses.

* Corresponding author. Fax: +1 619 5347190; e-mail: astockman@ucsd.edu.

The visual stimulus shown in the top panel of Fig. 1 is the primary stimulus used in all but one of the experiments described below. Rather than using continuously-presented sinusoidal-flicker, however, we modulated its amplitude sinusoidally. We refer to the sinusoidal carrier frequency as f_c and its amplitude-modulation frequency as f_{am} (see Eq. 2, below). In our experiments, f_{am} was always lower in frequency than f_c . Such stimuli are composed of only higher frequency sinusoidal components at or near f_c , as indicated by the arrow in the second panel of Fig. 1, there being no sinusoidal component at f_{am} (in fact, the higher frequency components are the carrier frequency, f_c , and two sidebands, $f_c - f_{am}$ and $f_c + f_{am}$, with relative amplitudes of 0.50:0.25:0.25, respectively; see Eq. 3, below). Since the late temporal filter shown in Fig. 1 blocks higher frequencies near f_c , it blocks the flickering stimulus, passing only the time-average signal. This system, therefore, obeys the Talbot–Plateau law.

Fig. 2 shows a simplified nonlinear model of the visual system that fails to obey the Talbot–Plateau law. This model differs from the linear model of Fig. 1 in only one respect: a compressive nonlinearity (Fig. 2, third panel), has been interposed between the early and

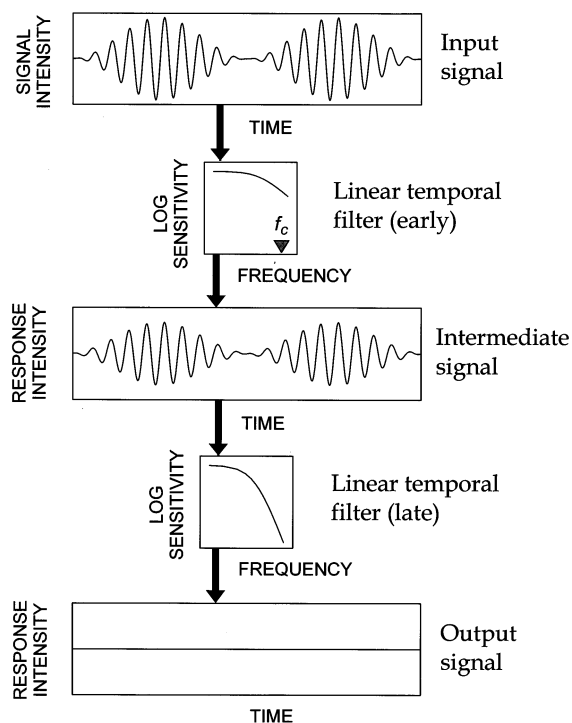


Fig. 1. Simplified linear model of the visual system. Top panel: input signal, two cycles of amplitude-modulated sinusoidal flicker. Second panel: early linear temporal filter that transmits f_c (arrow labeled f_c). Third panel: intermediate signal. Fourth panel: late linear temporal filter that severely attenuates f_c , but not low frequency sinusoidal flicker. Bottom panel: output signal. Since the intermediate signal is composed of high-frequency components alone, which are blocked by the late temporal filter, the output is steady.

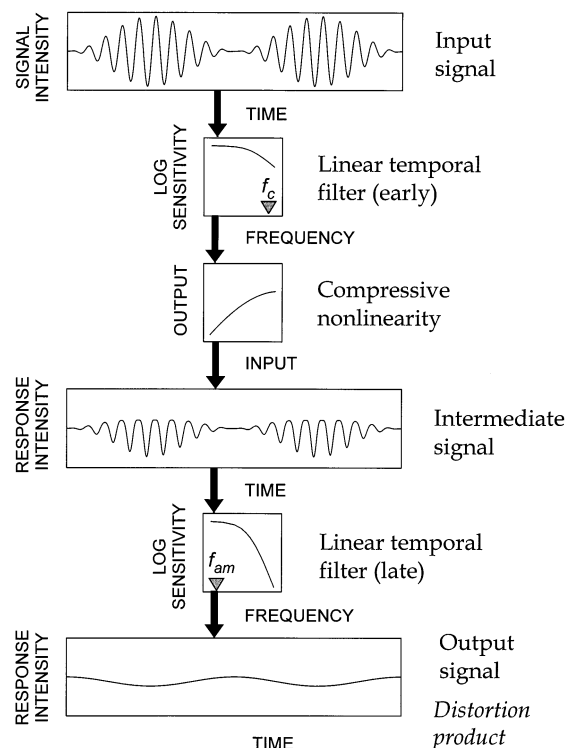


Fig. 2. Simplified nonlinear model of the visual system. Top panel: input signal, as Fig. 1. Second panel: early temporal filter, as Fig. 1. Third panel: compressive nonlinearity. Fourth panel: intermediate signal. Fifth panel: late temporal filter, as Fig. 1, that severely attenuates the sinusoidal carrier frequency (arrow labeled f_c in second panel), but not the low-frequency distortion at f_{am} (arrow labeled f_{am}). Bottom panel: output signal. The compressive nonlinearity produces a low-frequency component at f_{am} , which is transmitted by the late temporal filter.

late linear filters. Passing amplitude-modulated flicker signal through this nonlinearity compresses the peaks of the signal and produces a low frequency sinusoidal component at f_{am} (and smaller components at higher harmonics of f_{am}) that are not present in the original stimulus. When the compressed signal is passed through the late temporal filter, frequencies near f_c are again blocked, as in the linear model of Fig. 1. Yet, in this case, the low-frequency signal produced by distortion at f_{am} , which is indicated by the arrow in the penultimate panel, is transmitted to yield the slowly-changing output signal shown in the final panel. In contrast to the linear system of Fig. 1, the nonlinear system of Fig. 2 does not obey the Talbot–Plateau law. Any flicker signal that is transmitted by the early filter to reach the nonlinearity will produce a lower average output signal than a steady signal of the same average intensity, irrespective of whether the flicker signal is transmitted by the late filter.

The main advantage of using amplitude-modulated flicker is that it produces a distortion signal at f_{am} . Thus, we can independently manipulate f_c , which alters the sensitivity of stages before the nonlinearity to the

stimulus, and f_{am} , which changes the frequency or frequencies of any changes produced by distortion after the nonlinearity.

Under most conditions of adaptation, the Talbot–Plateau law appears to hold. Under the conditions of our experiment, however, it does not: a sinusoidally-flickering S-cone-detected target looks more yellow than a steady target, even when the flicker is above the observer’s CFF [75]. This failure of the Talbot–Plateau law implies that in the S-cone pathway, as in the model illustrated in Fig. 2, a substantial nonlinearity precedes the stage or filter that limits flicker detection. Such a nonlinearity is important because the distortion that it produces can be used to distinguish the temporal characteristics of the visual pathway before and after the nonlinear site: that is, we can separately determine the properties of the early and late temporal filters illustrated in Fig. 2. Considering the visual system as a triple ‘sandwich’ of linear, nonlinear, and linear stages [15] that can be separated by analyzing nonlinear distortion is now a relatively common research strategy. Such studies typically analyze the nonlinear interactions between stimuli of two or more sinusoidal frequencies (as in this study) or interactions within white noise [16–24]. The novel feature of this study is that our newly discovered failure of the Talbot–Plateau law can be used to measure the distortion in the perceptual absence of the flicker that produces it.

To learn more about the nonlinearity, we also carried out a series of nulling experiments, in which we canceled, with sinusoidal flicker, the color change produced by the distortion of the amplitude-modulated flicker. These results confirmed that the nonlinearity is compressive, and demonstrated that the function relating input modulation to output distortion is closer to a linear function than the quadratic function expected of most smooth compressive nonlinearities [25]. We argue that the nonlinearity is a ‘hard’ one (i.e. one with an abrupt change in its input–output function) that probably reflects an abrupt clipping of the S-cone signal above certain signal levels (see Fig. 13, below).

2. Methods

2.1. Apparatus

The optical apparatus was a five-channel, Maxwellian-view system illuminated by a 900-W Xenon arc light source. Test and field wavelengths were selected by the use of interference filters (Ealing and Oriol). IR and UV radiation were minimized by glass filters (Schott). The radiance of each beam was controlled by fixed and variable neutral density filters (Inconel). In addition, sinusoidal and other temporal waveforms were produced by pulse-width modulating

liquid-crystal light shutters (Displaytech) around a carrier frequency of 400 Hz. Each shutter had rise and fall times of $< 50 \mu\text{s}$, and could produce sinusoidal modulations from 0 to 90%. Modulation is defined as:

$$\frac{I_{\max} - I_{\min}}{I_{\max} + I_{\min}} \quad (1)$$

where I_{\max} is the maximum radiance and I_{\min} the minimum. Varying modulation varies the fraction of the light that is flickering, but not its time-average radiance. Modulation sensitivity, which is plotted in many of the figures below, is the reciprocal of the modulation threshold. The contrast of the shutter in the primary test channel measured in situ was better than 140:1 at 440 nm, 230:1 at 470 nm and 300:1 at wavelengths > 500 nm. The variability in contrast with wavelength has only a minimal effect on the modulation depth produced by pulse-width modulation. The optical waveforms were monitored periodically with the use of a Pin-10 photo-diode (United Detector Technology) linear amplifier, and oscilloscope. The observer’s head was stabilized by a rigidly-mounted dental wax impression.

2.2. Stimuli

In most experiments, a 440 nm flickering target of between 9.48 and 9.58 \log_{10} quanta $\text{s}^{-1} \text{deg}^{-2}$ (1.85 and 1.95 \log_{10} photopic trolands [ph td]) was presented in the center of a 620 nm background of 11.59 \log_{10} quanta $\text{s}^{-1} \text{deg}^{-2}$ (5.03 \log_{10} ph td). These conditions are known to produce good short-wave cone isolation [26], but we carried out further isolation controls (see Fig. 4 below). In some experiments, an additional 609-nm target of 11.03 \log_{10} quanta $\text{s}^{-1} \text{deg}^{-2}$ (4.61 \log_{10} ph td) or a 640-nm light of 11.07 \log_{10} quanta $\text{s}^{-1} \text{deg}^{-2}$ (4.16 \log_{10} ph td) was added to stimulate the longer wavelength, L- and M-cones. These conditions cause little or no bleaching of the S-cone photopigment. All stated radiances are time-average. The targets and background field subtended 4 and 9° diameter of visual angle, respectively. In most experiments, amplitude-modulated flicker was used (see the upper panels of Figs. 1 and 2). In the forced-choice experiment, however, a single cycle of the amplitude-modulated flicker was presented in one of two alternative temporal intervals. The intensity of the 440-nm target was systematically varied in the critical flicker fusion experiments.

The amplitude-modulated waveform was:

$$R \{1 + m \sin(2\pi f_c t)[0.5 + 0.5 \cos(2\pi f_{am} t)]\} \quad (2)$$

where R is the target radiance, m the modulation (0–0.9), f_c the carrier frequency (Hz), f_{am} the amplitude-modulation frequency (Hz), and t is time (s). An alternative way of writing Eq. 2, which emphasizes the frequency content of the waveform, is:

$$R[1 + m \{0.5 \sin(2\pi f_c t) + 0.25 \sin[2\pi(f_c - f_{am})t] + 0.25 \sin[2\pi(f_c + f_{am})t]\}] \quad (3)$$

2.3. Subjects

Three male (AS, DJP, PW) and one female (CK) subjects were used in these experiments. Two were experienced, well-trained subjects (AS, DJP), and two were relatively inexperienced (CK, PW). All had normal color vision and required no corrective lenses.

2.4. Calibration

The radiant fluxes of test and background fields were measured in the plane of the observer's entrance pupil with a radiometer (Graseby) that had been calibrated by the manufacturer against a standard traceable to the US National Bureau of Standards, and cross-calibrated by us against other devices traceable to both US and German standards. Neutral density filters were calibrated in situ for all test and field wavelengths used. Interference filters were calibrated in situ with a spectroradiometer (E,G and G).

We carried out both physical and psychophysical tests of system linearity. Measured with an integrating radiometer, the difference in time-average radiance between 90% modulated flicker and 0% modulated flicker of up to 40 Hz (the highest frequency used) was $< 0.2\%$ of the average radiance. Under the conditions of our experiments, any distortion signal produced by the apparatus is therefore well below S-cone threshold (see Section 3). The lack of visible distortion produced by the apparatus was confirmed in a psychophysical test of linearity, which is described below (see Section 3.1.2). Other physical tests, carried out with the use of filters to isolate different frequency bands, confirmed that the frequency content of our stimuli was correct.

2.5. Procedures

Subjects interacted with the computer by means of an eight button keypad, and obtained feedback by means of tones and a voice synthesizer.

Continuously-presented, amplitude-modulated flicker could produce the percept of a slow color change at f_{am} and bursts (at intervals of $1/f_{am}$) of high frequency flicker. We measured the thresholds for both using the method of adjustment. Data were averaged from at least four or five runs.

2.5.1. Flicker thresholds

To set modulation thresholds for flicker, subjects varied the modulation depth of the amplitude-modulated sinusoidal flicker until they were satisfied that the perception of flicker, which they saw as bursts of high

frequency flicker, was just at threshold. Subjects could adjust the modulation up or down in steps of 0.02 or $0.10 \log_{10}$ unit using different keys. They were instructed to respond only to the high frequency flicker and to ignore any slow color change that might also be present. In some experiments, f_c was manipulated, in others f_{am} was manipulated.

To set critical flicker fusion frequencies for flicker, subjects adjusted f_c with f_{am} fixed at 0.5-Hz until the perception of flicker was just at threshold. The modulation m in all CFF measurements was set at the maximum value of 90%.

2.5.2. Color thresholds

To set modulation thresholds for color, subjects varied the modulation of the amplitude-modulated sinusoidal flicker until they were satisfied that the perception of a slow color change at f_{am} was just at threshold. In this case, subjects were instructed to respond only to the slow color change, and to ignore the bursts of high frequency flicker. Again, in some experiments, f_c was manipulated, while in others f_{am} was manipulated.

To set critical color fusion frequencies for color, subjects adjusted f_c with f_{am} fixed at 0.5 Hz until the slow 0.5-Hz color change was just at threshold.

The color changes produced by amplitude-modulated flicker were subtle—particularly near-threshold, where threshold settings were difficult to make. Experienced subjects, however, were able to make precise, repeatable color threshold settings. Inexperienced subjects were less reliable, but could consistently judge the relative sensitivity to color and flicker.

2.5.3. Forced-choice

For the experiments in which f_{am} was fixed at 0.5 Hz and f_c manipulated, we augmented the method of adjustment with a temporal two-alternative forced-choice procedure. For DJP, whose color thresholds always lay well below his flicker modulation thresholds, the forced-choice procedure probed sensitivity to the slow color change. For AS, the forced-choice procedure probed sensitivity to the slow color change at higher temporal frequencies, and to flicker at lower temporal frequencies.

Instead of continuously-presented amplitude-modulated flicker, for the forced-choice procedure we presented a single cycle of 0.5-Hz amplitude-modulated flicker (i.e. raised-cosine-windowed flicker) in one of two alternative, 1 s intervals, and no flicker in the other interval. The intervals were delimited at their beginning and end by two different tones, and the interval within which the flicker was presented was randomly varied between trials. Following both intervals, the subject indicated which interval contained the stimulus by pressing one of two buttons. Dual randomly interleaved staircases were used. Independently on each staircase,

the modulation on the next trial was raised whenever the subject made an incorrect response on the current trial and decreased whenever he made two correct responses in a row, so that the staircases converged on 70.7% correct. The stepsize was 0.05 \log_{10} unit. Thresholds were averaged from sixteen reversals of staircase direction (eight reversals on each of the two staircases). A ‘ballpark’ procedure, which was designed to provide a preliminary estimate of the threshold level, preceded data collection. This ballpark estimate was used as the starting modulation for the two forced-choice staircases.

Presenting a single cycle of amplitude-modulated flicker, rather than continuously-presented amplitude-modulated flicker, has the effect of smearing the frequency content of the stimulus and thus of the low frequency distortion that is produced. For example, distorting a single cycle of 0.5-Hz amplitude-modulated flicker (according to the ceiling model introduced below, with the mean S-cone signal level at the level of the ceiling, see Fig. 13, example 2) produces a band of low frequency signals ranging from 0 to ~ 1 Hz, whereas distorting continuously-presented 0.5-Hz amplitude-modulated flicker produces discrete signals at 0 and 0.5 Hz. Such differences should have relatively little effect in experiments in which f_{am} is fixed and f_c varied, other than changing overall sensitivity.

2.5.4. Flicker nulls with phase adjustments

Flicker nulls were achieved by adjusting the relative phase and modulation of two superimposed flickering targets until their flicker signals canceled each other, and they appeared steady. Modulation was continuous. Two types of flicker nulls were set, as follows:

2.5.4.1. Nulling the colored distortion product. Subjects were presented, as before, with the amplitude-modulated S-cone-detected 440-nm target presented on the 620-nm background. A second 440-nm target, which was half the radiance of the first, was then superimposed and sinusoidally flickered at f_{am} . The combined target radiance was set to the standard radiance for a single 440-nm target (see above). The addition of the second target slightly reduced the largest amplitude-modulation that could be produced. Each subject’s task was to adjust the phase and modulation of the new target to cancel the slow color change produced by distortion at f_{am} .

Subjects could advance or retard the phase of the sinusoidal flicker relative to the amplitude-modulation in steps of 2 or 10° using four different keys. Using a fifth key they also had the option of reversing the relative phase of the two stimuli by 180°. This last option proved useful for quickly finding the correct phase for cancellation. If the relative phase was close to the correct one for cancellation, the flicker percept

increased markedly when the phase was reversed, whereas if it was close to 180° away from the correct one, it decreased markedly. In contrast, if the phase was $\pm 90^\circ$ away from the cancellation phase, the flicker percept changed little when the phase was reversed. Subjects also adjusted the modulation of the sinusoidally flickering stimulus to complete the null. The results are averaged from ten or more settings.

2.5.4.2. Nulling the amplitude-modulated flicker. In other experiments, we nulled amplitude-modulated S-cone flicker with amplitude-modulated L- and M-cone flicker. Subjects were again presented with the S-cone-detected 440-nm target presented in the center of the intense 620-nm background. A 609-nm target was superimposed on the violet target to provide L- and M-cone-detected flicker. To find the optimal relative phase and modulation for a null between the S-cone and L/M-cone flicker, we used continuously-presented sinusoidal flicker. Continuous flicker made the task much easier for the subjects, and produced settings that yielded cancellation that was as good when amplitude-modulated flicker was used. At each frequency (usually 10–40 Hz), subjects were presented with the S-cone light and the L/M-cone light. Initially, the modulation of each was approximately twice the modulation threshold and the relative phase was 180° (i.e. in opposite phase).

Each subject’s task was to set a flicker null by adjusting both the phase difference between the two lights and their relative modulation depths. The method that was used was similar to the one described in the previous section to cancel the distortion product. Since nulling the distortion product was carried out at low frequencies ($f_{am} = 0.5$ –5 Hz), whereas nulling the amplitude-modulated flicker was done at moderate to high frequencies ($f_c = 10$ –40 Hz), the two tasks were subjectively very different.

The reason for finding the best null between S-cone flicker and L/M-cone flicker was so that we could then present the two stimuli together, amplitude-modulated in phase at 0.5 Hz, with their carrier frequencies fixed at the optimal relative phase and modulation for flicker cancellation. To our surprise, when we did this, we found that subjects could still see the slow 0.5-Hz color change, even though they could not see the S-cone flicker, since it was nulled by L/M-cone flicker (see Fig. 10). Thus, by adding the canceling L/M-cone stimulus, we could null the S-cone flicker, yet still measure the sensitivity to the slow color change. This experiment is described further below (see Section 3.5).

2.5.5. Beat measurements

Another method can be used to probe S-cone temporal sensitivity beyond the S-cone temporal resolution limit. Stockman et al. [14] found that sub-threshold

S-cone flicker of up to ~ 40 Hz can interact with supra-threshold L- or M-cone flicker of a slightly different frequency to produce beats at the difference frequency (e.g. a 40-Hz S-cone and a 39.5-Hz L-cone stimulus will produce a 0.5-Hz beat). To allow direct comparisons with our color distortion data, we made S-cone beat-sensitivity measurements under the same stimulus conditions as used in our main experiment.

Subjects were presented with the S-cone-detected 440-nm target, and an L/M-cone-detected 640-nm target, superimposed in the center of the intense 620-nm background. Both were continuously flickered—they were not amplitude-modulated. To measure the temporal characteristics of the S-cone beat interaction with L/M-cone stimuli, we covaried the temporal frequency of the flickering components—keeping them 0.5 Hz apart in frequency—and measured the S-cone modulation required for the beat to be just detectable. The modulation of the L/M-cone flicker was maintained slightly supra-threshold ($\sim 0.2 \log_{10}$ unit above threshold) at all frequencies. Again, the method of adjustment was used. The beat, which was produced by the interaction between two continuously-flickering stimuli, was seen as a 0.5-Hz modulation of the amplitude of the suprathreshold L/M-cone flicker. No slow 0.5-Hz color change was seen, because the interaction between the S- and L/M-cone flicker that causes the beat occurs after the nonlinearity in the S-cone pathway (see below).

3. Results

Under most conditions of adaptation the Talbot–Plateau law appears to hold [27,28] but see for example [76]. It does not hold, however, under the conditions of our experiment, which were chosen to ensure that the S-cones mediate flicker detection. For three out of four subjects, we found that S-cone flicker was accompanied by a shift in the perceived target color towards yellow, even when the flicker rate was above CFF or when the flicker modulation was below threshold (see below). A change in color towards yellow (i.e. less blue) suggests that there is an apparent decrease in the time-averaged S-cone level when the light is flickered, and therefore that the nonlinearity is compressive.

3.1. Basic findings

3.1.1. Color and flicker modulation sensitivities

In the first experiment, we measured separately the thresholds for the slow color change and for the flicker bursts in four subjects. Subjects were each presented with a series of stimuli that varied in f_c from 5 to 40 Hz but had a fixed f_{am} of 0.5 Hz. At each f_c , the subject's task was to adjust the flicker modulation until the slow

color change at 0.5 Hz was just at threshold. Conversely, in a separate experiment, the task was to adjust the flicker modulation until the bursts of flicker also at 0.5 Hz were just at threshold.

The results for AS, CK, DJP and PW are shown in Fig. 3. The S-cone modulation thresholds for detecting the 0.5-Hz color change are shown by the open circles and those for detecting the flicker are shown by the filled circles. The error bars are ± 1 S.E. The regions within which the Talbot–Plateau law fails (i.e. when the slow color change can be seen but the flicker cannot) have been shaded.

For AS, there is an extensive region above ~ 20 Hz within which the slow color change can be seen, but the flicker cannot, and, beyond 30 Hz, a region within which only the color change can be seen. For DJP, who is less sensitive than AS to S-cone flicker (see also Fig. 15), the slow color change can be seen in the absence of flicker at all frequencies, and beyond 20 Hz only the color change can be seen. For CK, the most inexperienced subject, the flicker and color thresholds are similar at all frequencies, except for the small region above 30 Hz, where the subject consistently reported seeing color in the absence of flicker. The three shaded regions constitute violations of the Talbot–Plateau Law. Our fourth subject, PW, also saw the color change, but only in the presence of flicker.

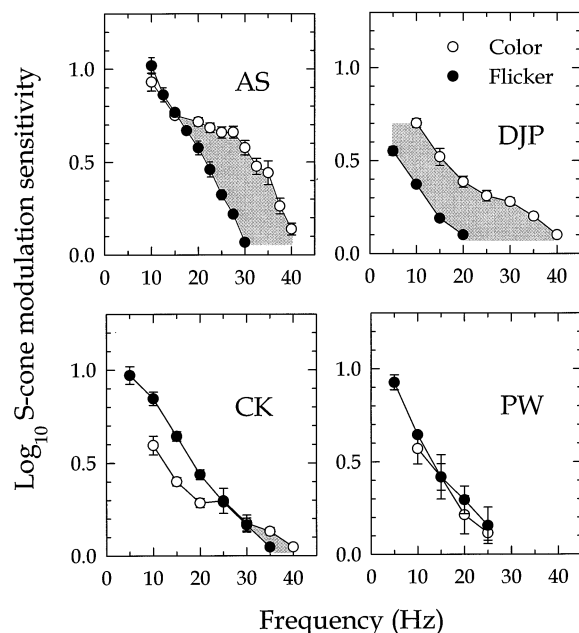


Fig. 3. \log_{10} modulation sensitivities for seeing bursts of flicker (filled circles) or seeing a color change (open circles) at f_{am} as a function of carrier frequency, f_c . The data for AS are shown in the upper left panel, for DJP in the upper right panel, for CK in the lower left panel and for PW in the lower right panel. The shaded regions indicate those carrier frequencies and modulations for which the Talbot–Plateau Law fails: i.e. where a color change is seen in the absence of flicker. The error bars in all figures are ± 1 S.E.

The results for these subjects show that there can be large individual differences in the sensitivities for seeing color and for seeing flicker. Consequently, some subjects, such as AS and DJP, show an impressive and unmistakable failure of the Talbot–Plateau law, while others, such as CK and PW, show a much smaller effect or no effect. In the remainder of the experiments, we concentrated on testing DJP and AS, for whom the color and flicker modulation thresholds were well separated.

3.1.2. Test of linearity

To be certain that the nonlinear distortion is produced entirely within the S-cone pathway, we needed to ensure that the experimental apparatus itself was free of significant distortion. We confirmed that the apparatus was linear to within 0.2% (see Section 2), but, as an additional control, we carried out the following psychophysical test, which showed that any distortion produced by the apparatus was visually insignificant.

We first measured S-cone spectral sensitivity at 440 and 470 nm for AS and DJP. Both subjects set flicker thresholds for continuously-presented, 90% modulated 1, 5 and 10-Hz flicker superimposed on the 620-nm background by adjusting the radiance of the targets. The spectral sensitivities, which were independent of frequency, were averaged. We used the mean spectral sensitivity for each subject to equate 470 and 440-nm targets for their effects on the S-cones. Using the 440-nm light, we then remeasured the thresholds for seeing the slow, 0.5 Hz color change, as before, by varying f_c from 10 to up to 40 Hz with a fixed f_{am} of 0.5 Hz (as in the previous experiment), and contemporaneously, we measured the same function using the S-cone-equated 470-nm light. We found that the 440 and 470-nm functions (results not shown) roughly superimpose for AS and DJP. Subjectively, the 440 and 470-nm experiments were indistinguishable, and, importantly, the color change towards yellow coincided with the flicker bursts at both wavelengths. Thus, if the distortion originates in the experimental apparatus, its effect is similar in the two optical channels that produce the 440 and the 470-nm stimuli (conceivably, the distortion could have had opposite effects in the two optical channels, so that the distortion products canceled when the two lights were combined).

The crucial test of linearity was to combine the 440 and 470-nm lights, with their amplitude-modulation frequencies in-phase, but their sinusoidal carrier frequencies in opposite phase, and then repeat the measurements. Since the two lights are S-cone-equated, the flicker should cancel at the S-cone photoreceptor, and no flicker or color distortion should be seen whatever the form of the S-cone nonlinearity. If the distortion is produced in the experimental apparatus, however, the slow color change should still be visible. We found that

the subjects were unable to detect a color change at any frequency. Thus, we conclude that the nonlinearity is in the visual system.

3.1.3. Color and flicker CFFs

In preliminary experiments, we found that the highest f_c up to which a visible distortion signal could be seen was strongly dependent upon the radiance of the 440-nm target. Consequently, before most experiments, we carried out a pilot experiment to determine the 440-nm radiance that maximized the visibility of the distortion product. To investigate the dependence of distortion on the S-cone excitation level more formally and to determine the range of levels over which the violation of the Talbot–Plateau law is found, we carried out the following critical flicker fusion experiments, the results of which are shown in Fig. 4.

The leftmost data set in the upper panel of Fig. 4 (circles) shows, for a fixed f_{am} of 0.5 Hz, the effect of varying the 440-nm target radiance on the highest f_c at which a 0.5-Hz color change (open symbols) or a 0.5-Hz flicker burst (filled symbols) could just be seen. For brevity, we will refer to these as the color CFF and the flicker CFF, respectively. Comparable data for DJP are shown in the lower right panel of Fig. 15. For both subjects, the color CFF function is triangular in shape, reaching a peak at 9.85 (AS) and 9.28 (DJP) log quanta $s^{-1} \text{ deg}^{-2}$, and falling steeply at lower and higher radiances. The flicker CFF function is similar to previous S-cone CFF measurements made with continuously-presented flicker [26,29]: it grows roughly linearly with log radiance, in accordance with the Ferry–Porter law [30,31], until reaching a plateau at 23 Hz (DJP) or 29 Hz (AS), after which it saturates, before rising once again at still higher radiances.

To determine the cone types that mediate the flicker and color CFFs, we repeated the CFF measurements for AS at three additional target wavelengths: 461 nm (inverted triangles); 490 nm (squares) and 560 nm (triangles), which are also shown in the upper panel of Fig. 4 (so as not to overlap, these functions have been separated horizontally). Changing the wavelength of the target dramatically alters the shape of the flicker CFF functions. Nonetheless, we can account for all the functions by laterally displacing two shape-invariant template curves, one of which we attribute to detection by S-cones, and the other to detection by M-cones. The color CFF functions, in contrast, can be accounted for by displacing a single template curve.

We can infer the cone type that determines the CFF from the changes in sensitivity that accompany changes in the target wavelength. If the CFF functions in the upper panel are laterally shifted to compensate for changes in S-cone spectral sensitivity, those portions of the curves that then overlie are likely to be determined by the S-cones (and similarly for the M-cones). The

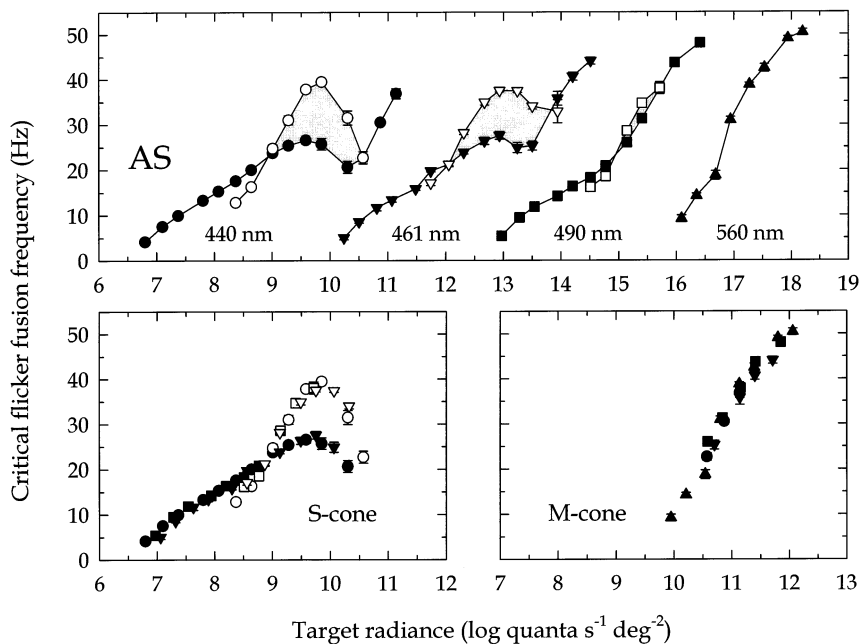


Fig. 4. The upper panel shows flicker (filled symbols) and color (open symbols) CFF data for AS measured at target wavelengths of 440 (circles), 461 (inverted triangles), 490 (squares) and 560 nm (triangles) as a function of target radiance. The shaded areas show the radiances and frequencies for which the Talbot–Plateau law fails. For clarity, the functions in the upper panel have been shifted laterally by 3.00 \log_{10} units at 461 nm, 6.00 \log_{10} units at 490 nm, and 7.20 \log_{10} units at 560 nm. The radiance scale along the abscissa is correct for the 440 nm targets in all three panels. In the lower left panel, the functions have been shifted laterally by $-0.18 \log_{10}$ units at 461 nm, $-0.80 \log_{10}$ units at 490 nm, and $-3.24 \log_{10}$ units at 560 nm. These shifts equate the targets of different wavelength for their effects on the S-cones to the effect of the 440-nm target. In the lower right panel, the functions have been laterally shifted by 0.20 \log_{10} units at 461 nm, 0.64 \log_{10} units at 490 nm and 1.06 \log_{10} units at 560 nm. These shifts equate the targets of different wavelength for their effects on the M-cones to the effect of the 440-nm target. M-cone spectral sensitivities: Stockman et al. [73]. S-cone spectral sensitivities: individual (AS) and group measurements from Stockman et al. [74].

symbols in the lower left panel show the portions of the four CFF functions that overlie each other once the targets have been S-cone-equated. The color CFF and most of the flicker CFF, except for the final rising portion, are determined by the S-cones. The symbols in the right lower panel show the portions of the CFF functions that overlie once the targets have been M-cone-equated. The steeply rising portion of the CFF is determined by the M-cones.

Below, we present a simple model that can account for the shapes of both the S-cone color and flicker CFF curves.

3.2. Canceling the distortion product with real S-cone flicker

The color change that accompanies amplitude-modulated flicker can be canceled by a second S-cone-detected light that is sinusoidally-flickering at f_{am} and adjusted appropriately in relative phase and modulation depth. The phase advance of the sinusoidal flicker required to null the color change (relative to the amplitude-modulation and sinusoidal-modulation being in opposite phase) are shown in Fig. 5, plotted as a function of f_{am} for AS (filled circles) and DJP (open circles). For both subjects, f_c was fixed at 25 Hz. The

addition of the second S-cone light reduced the largest possible amplitude-modulation. Thus, although 25 Hz is below the flicker CFF for AS, he saw little or no flicker even at the highest modulations used in this and the following experiment.

The results for AS and DJP lie near to a phase lag of 180° (horizontal line), at which the high modulation of the amplitude-modulated flicker and the sinusoidal-modulation of the low-frequency flicker are in phase (see icons, right). Thus, the color change associated with the flicker burst is canceled by an increase in the S-cone light, a result which confirms that the nonlinearity is compressive.

The distortion signal after the nonlinearity will inherit any delays to the high frequency components that are introduced by stages before the nonlinearity. If the delays before the nonlinearity are independent of frequency (i.e. similar to a time delay, so that all frequency components are delayed by the same time), phase lags of 180° at all frequencies would be expected, since the high frequency components making up the stimulus waveform (at $f_c - f_{am}$, f_c and $f_c + f_{am}$) and the canceling low frequency sinusoids (at f_{am}) would be equally delayed. Yet, although the data of Fig. 5 lie roughly parallel to the abscissa, they fall on average about 20° above 180° . We are uncertain about the

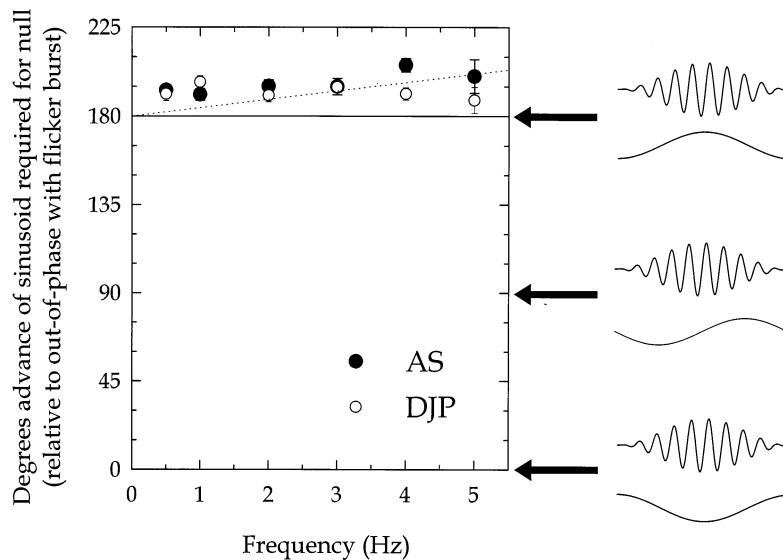


Fig. 5. Degrees advance of sinusoidal flicker for AS (filled circles) and DJP (open circles) needed to null the color change produced by amplitude-modulated flicker are shown as a function of amplitude-modulation frequency, f_{am} . The advances are relative to the sinusoidal modulation being in opposite phase with the amplitude modulation. The dotted line is a model prediction (see text for details). The drawings on the right show the amplitude-modulated flicker and sinusoidal flicker at relative phase differences of 0, 90 and 180°.

cause of this offset. If the delay of the high frequency components were different from the delay at lower frequencies, we would expect the phase lags to increase or decrease with frequency. An example of such a function is illustrated by the dotted line in Fig. 5, which has a best-fitting slope of $4.5^\circ \text{ Hz}^{-1}$. Such a slope suggests that, relative to any common time delay, the low frequency sinusoid is delayed by 12.5 ms more than the high frequency components.

In a separate experiment, we measured in AS similar phase lags, but as a function of f_c (15–35 Hz) for a fixed f_{am} of 0.5 Hz. Since we found no change in the phase lag with f_c , these results are not shown.

The ability to cancel the distortion product with real flicker provided a means of measuring the relation between input modulation and output distortion for the nonlinearity, a knowledge of which was required in order to estimate the frequency response after the nonlinearity (see below). Subjects were asked to null the output distortion as a function of input modulation of the amplitude-modulated flicker. An f_c of 25 Hz and an f_{am} of 0.5 Hz were used. The results for AS (top panel) and DJP (bottom panel) are shown in Fig. 6 as dotted circles. The dashed lines are the best-fitting quadratic functions. A large quadratic component is expected from most continuous or smooth compressive nonlinearities [25]. For both subjects, but more clearly for DJP, the results lie closer to a linear relationship than to a quadratic one. The solid lines, which are constrained to pass through the origin, have best-fitting linear slopes of 0.082 and 0.098 for AS and DJP, respectively. For AS, the data are better described by the dotted line, which crosses the ordinate at a cancel-

ing modulation of -0.007 and has a linear slope of 0.098. The linear relationship between the input modulation and output distortion led us to propose the ceiling model, which is introduced in Section 4.3, below. This model can also account for the non-zero intercept found for AS.

In these experiments, the modulation of the sinusoidal flicker required to cancel the color change was too low for the canceling flicker to produce a visible distortion product.

3.3. The temporal frequency response before the nonlinearity: the early filter

We used the nonlinear distortion to probe the temporal sensitivity of the S-cone pathway both before and after the nonlinear site at which the distortion occurs. To measure the properties of the stages before the nonlinearity, we measured the subjects' sensitivity to the slow color change as a function of f_c for a fixed f_{am} of 0.5 Hz. This technique determines the temporal sensitivity of the stages before the nonlinearity, and thus provides an estimate of the early temporal filter shown in Figs. 1 and 2. The stages after the nonlinearity can be discounted in this experiment, because, when the color threshold is lower than the flicker threshold, the later stages are always presented with the same stimulus (a threshold 0.5-Hz color change) whatever the value of f_c . Consequently, the stages after the nonlinearity should not affect the measured sensitivities, which instead should depend only on the sensitivities of the stages before the nonlinearity to f_c (a signal at f_{am} is not, of course, present until after the nonlinearity).

In fact, the results of this experiment, obtained by the method of adjustment, have been shown previously for all four subjects as open circles in Fig. 3. Although the color changes produced by S-cone distortion were clearly visible above threshold, precise threshold settings using the method of adjustment were difficult even for experienced subjects. We therefore repeated our measurements for DJP and AS using forced-choice methods. The forced-choice results are shown in Fig. 7 (dotted symbols) for AS (upper panel) and DJP (lower panel). Near-threshold, AS reported seeing color without flicker above 15 Hz, whereas DJP reported seeing color without flicker at all frequencies.

Both methods of estimating the sensitivity for detecting the slow color change produce curves with roughly similar overall shape. In forced-choice, the subject must choose which of two temporal intervals contains the color change, rather than decide whether or not the color change is visible. The forced-choice measurements are consequently less dependent on the subject's threshold criteria, and should therefore more accurately reflect the underlying temporal sensitivity function. The forced-choice results for AS and DJP are similar in

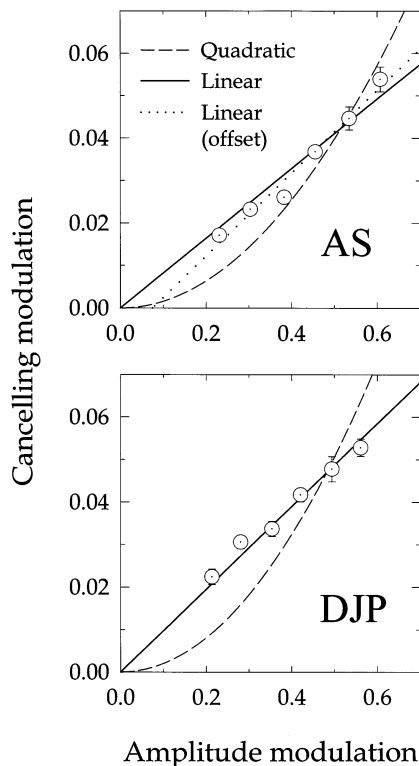


Fig. 6. S-cone modulations required to cancel the color change produced by amplitude-modulated flicker (dotted circles) for AS (upper panel) and DJP (lower panel) as a function of the depth of amplitude modulation. Also shown are the linear (solid lines) and quadratic (dashed lines) functions best-fitting the data and constrained to pass through the origin, and for AS the linear function (dotted line) best-fitting the data and not constrained to pass through the origin.

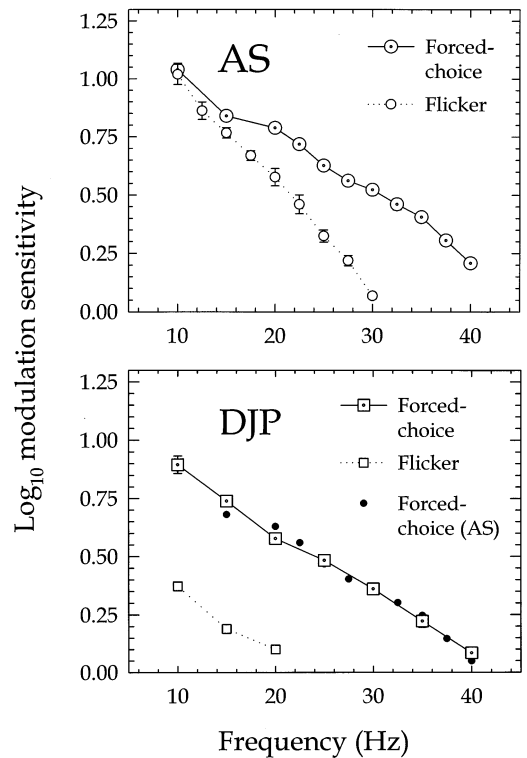


Fig. 7. Log_{10} temporal modulation sensitivities for AS (upper panel) and DJP (lower panel) measured by the method of adjustment for seeing bursts of flicker (open circles, AS and squares, DJP) at an f_{am} of 0.5 Hz, and forced-choice thresholds for detecting a single cycle of 0.5-Hz amplitude-modulated flicker (dotted circles, AS and squares DJP) both plotted as a function of f_c . The forced-choice data for AS are shown again in the lower panel (filled circles) vertically aligned with the data for DJP.

shape. For comparison, the results for AS are also shown in the lower panel of Fig. 7 (filled circles) vertically aligned with the results for DJP.

The sensitivity function for detecting the color change extends to much higher frequencies than that for directly detecting flicker. The simplest explanation of this finding is that the nonlinearity is comparatively early in the S-cone pathway, so that the sensitivity measured up to the nonlinearity is less subject to transmission losses than conventional measures, which probe the sensitivity of the pathway both before and after the nonlinearity.

3.4. The temporal frequency response after the nonlinearity: the late filter

To estimate the properties of the stages after the nonlinearity, we first measured the sensitivity to the slow color change as a function of f_{am} (0.5–5 Hz) for a fixed f_c (32.5 Hz for AS and 25 Hz for DJP). Since the stimuli for each subject had the same f_c , they should be equally attenuated by the early linear filter before the nonlinearity, yet produce color changes at the various

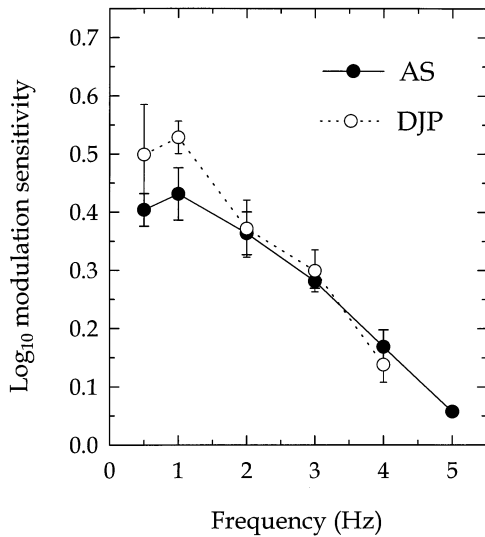


Fig. 8. Log_{10} temporal modulation sensitivities for AS (filled circles) and DJP (open circles) for seeing a color change as a function of f_{am} for a fixed f_c .

amplitude-modulation frequencies beyond the nonlinearity (see Fig. 2). The subjects' task, as in the previous experiment, was to vary the flicker modulation to find the threshold for the detection of the slowly changing distortion product. For AS and DJP, the sinusoidal flicker frequencies of 32.5 and 25 Hz, respectively, were above their flicker CFFs, so that flicker was never seen during this experiment.

Fig. 8 shows the result of varying for AS (filled circles) and DJP (open circles). Again, the error bars are ± 1 S.E. Notice that these functions are limited to ≤ 5 Hz. In Fig. 8, the sensitivity is plotted in terms of the stimulus modulation before the nonlinearity. In

order to calculate the actual sensitivity of the stages after the nonlinearity, we need to know how the slow color change after the nonlinearity ($m_{out(am)}$) depends on the stimulus modulation before the nonlinearity (m_{in}). The relevant functions, which were estimated by nulling the distortion product with real flicker, were shown in Fig. 6. To calculate the temporal sensitivity beyond the nonlinear site, we assumed the fitted linear function for DJP (solid line, Fig. 6, lower panel; $m_{out(am)} = 0.098m_{in}$) and the fitted offset linear function for AS (dotted line, Fig. 7, upper panel; $m_{out(am)} = 0.098m_{in} - 0.007$). The temporal sensitivities of the stages after the nonlinearity, and thus of the late temporal filter shown in Figs. 1 and 2, are shown by the open circles in Fig. 9. The data points in Fig. 9 shown as the filled squares are modulation sensitivities for directly-detected sinusoidal S-cone flicker.

Whereas the functions denoted by the open circles reflect the assumed temporal sensitivity of stages after the nonlinearity, those denoted by the filled squares represent the temporal sensitivity of the S-cone pathway as a whole. The differences between these two functions, therefore, should reflect the temporal properties of the S-cone pathway before the nonlinearity. As can be seen in Fig. 9, except at 0.5 and 1 Hz the two functions are very similar. At low frequencies, the directly measured temporal sensitivities exhibit a clear fall-off in sensitivity, whereas those after the nonlinearity do not. This finding suggests that the stages before the nonlinearity are bandpass. Indeed, the bandpass response is likely to be a property of the photoreceptors themselves [32]. These issues will be discussed further below (see Section 4 and Fig. 12).

In these experiments, the frequency content of the amplitude-modulated flicker varies with f_{am} . For AS, it

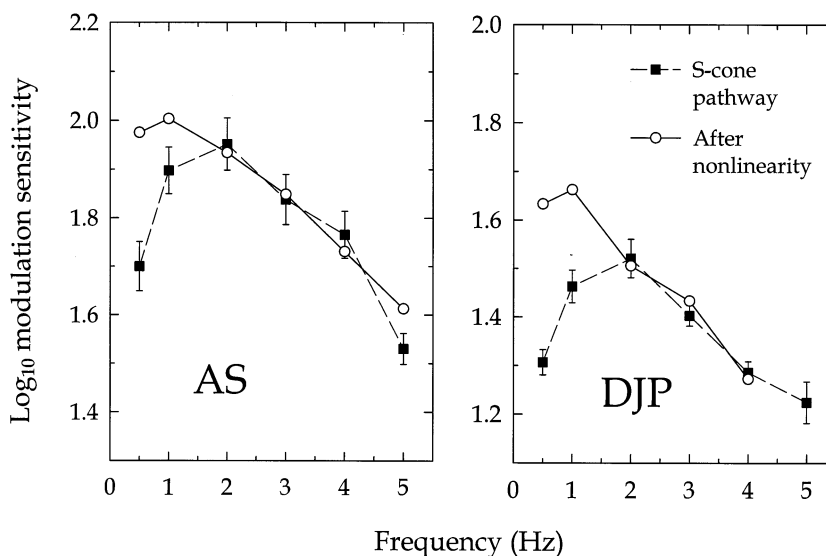


Fig. 9. Log_{10} temporal modulation sensitivities for AS (left panel) and DJP (right panel) for sinusoidal flicker (filled squares) compared with temporal sensitivity functions assumed to apply after the nonlinearity (open circles); both as are shown function of frequency.

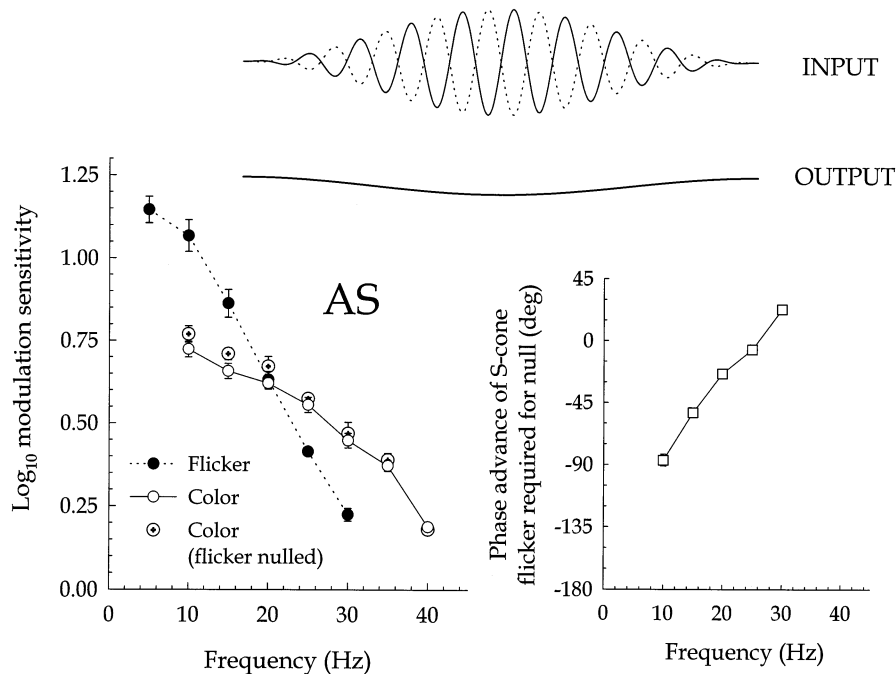


Fig. 10. Top panel: amplitude-modulated S-cone (solid line, INPUT) and L/M-cone flicker that is perceptually in opposite phase (dotted line, INPUT) are seen as a slow color change at the amplitude-modulation frequency (solid line, OUTPUT). Lower left panel: \log_{10} thresholds for seeing a flicker burst (filled circles) or a color change (open circles) at the amplitude-modulation frequency; and thresholds for seeing a color change (dotted circles) after the amplitude-modulated S-cone flicker has been nulled with amplitude-modulated L/M-cone flicker; both as a function of f_c . Right panel: phase advances of S-cone flicker, relative to opposite phase L/M-cone flicker, required to produce a flicker null as a function of f_c .

changes from $32 \oplus 32.5 \oplus 33$ to $27.5 \oplus 32.5 \oplus 37.5$ Hz; while, for DJP, it changes from $24.5 \oplus 25 \oplus 25.5$ to $21 \oplus 25 \oplus 29$ Hz (see Eq. 3) (the symbol \oplus represents superposition). Changing f_{am} , therefore, changes the frequencies of the two side bands. In those frequency ranges, the assumed temporal frequency response before the nonlinearity falls by $\approx 0.028 \log_{10}$ units Hz^{-1} (see Fig. 7, dotted symbols). Thus, the early filter increases the size of the lower sideband ($f_c - f_{am}$), and decreases that of the upper one ($f_c + f_{am}$), relative to the size of f_c . For DJP, the effect is no more than 1.29 and 0.77 times f_c for the lower and upper sidebands, respectively, even for his highest f_{am} of 4 Hz. For AS, the effect is larger since a higher f_{am} of 5 Hz was used, reaching 1.38 and 0.72 times f_c for the lower and upper sidebands, respectively. These relatively small changes are likely to have little effect on size of the distortion product at f_{am} , not only because they are small, but also because they are complementary. As we point out below, a complementary increase and decrease in the two sidebands leaves the distortion signal at f_{am} relatively unchanged (see Section 4).

3.5. Canceling the S-cone amplitude-modulated flicker with L- or M-cone flicker

For all but one subject (DJP), color threshold settings were made in the presence of suprathreshold

flicker at some frequencies (see Fig. 3). At those frequencies, there is a concern that the visible flicker might influence the color thresholds, perhaps in a frequency-dependent way, since the relative color and flicker sensitivities change with frequency.

We found that we could raise the flicker modulation threshold above the color modulation threshold by nulling the amplitude-modulated S-cone flicker with amplitude-modulated L- or M-cone flicker (which was produced by superimposing a $11.03 \log$ quanta $\text{s}^{-1} \text{deg}^{-2}$, 609-nm target on the 440-nm target). In fact, to our surprise, we found that nulling the amplitude-modulated S-cone flicker with amplitude-modulated L- or M-cone flicker canceled the perception of flicker, but had little or no effect on the visibility of the slow color change. This result is illustrated in the upper panel of Fig. 10. Amplitude-modulated S-cone flicker (top panel, INPUT, solid line) combined with amplitude-modulated L/M-cone flicker that was perceptually in opposite phase (top panel, INPUT, dotted line) together produce only a slow color change at f_{am} (top panel, OUTPUT, solid line).

In this experiment, f_{am} , the phase of the amplitude-modulation, and f_c were the same for both the S-cone and L/M-cone lights. In a preliminary experiment (see Section 2), we determined the relative phase of f_c and modulation of the two lights that produced optimal flicker cancellation. The lower right panel of Fig. 10

shows the phase settings for AS that produced the best cancellation. Consistent with previous work, S-cone flicker is delayed relative to the L/M-cone flicker, and, since the best cancellation phase tends towards the S-cone flicker actually being in phase with the L/M-cone flicker at 0 Hz, is inverted in sign relative to the L/M-cone flicker [26,33,34].

Following the preliminary settings, the S- and L/M-cone lights were presented together, fixed at each f_c at the phase lag and modulation ratio that produced the best cancellation. The subject then adjusted the modulations of both lights together (with the modulation ratio fixed) to find the target color threshold. The results for AS are shown as dotted circles in the lower left panel of Fig. 10. Concurrently, color thresholds (open circles) and flicker modulation thresholds (filled circles) were measured without the canceling L/M-cone flicker. The results obtained with flicker cancellation are very similar to those obtained without flicker cancellation, which suggests that suprathreshold S-cone flicker has little effect on the color threshold measurements.

The data in Fig. 10 for AS were measured about 3 years before those in Fig. 3. While the flicker modulation thresholds are similar in sensitivity, the later color thresholds are more sensitive than the earlier ones by about $0.1 \log_{10}$ unit. Small vertical shifts in the color distortion thresholds did occur between long experimental breaks, and we assume that they were due primarily to changes in the subjects' criteria. Small uncorrected drifts in target radiance, however, may also have influenced the thresholds, since, as the CFF results of Fig. 4 show, color thresholds can be very sensitive to small changes in radiance.

Canceling the amplitude-modulated S-cone flicker with L/M-cone flicker also had little effect on the color thresholds for DJP (data not shown), although for him the color modulation thresholds were always lower than those for flicker. The immunity of the colored distortion product from the cancellation of S-cone flicker by L/M-cone flicker reveals much about the postreceptoral organization of these signals. It suggests either that the S-cone flicker is not canceled by L/M-cone flicker until after the nonlinearity (see Fig. 16), or that the color change is produced by a nonlinearity in a pathway that is entirely separate from the one that signals flicker at 10 Hz and above. The modeling of the color and flicker CFF data shows that the changes in flicker and color sensitivity can be accounted for by a single nonlinearity (see Fig. 15 and below), which might therefore be common.

At the threshold for seeing the slow color change, the amplitude-modulated 609-nm flickering light needed to be only a small multiple of the L/M-cone flicker modulation threshold ($\sim 2 \times$ its threshold) to cancel the S-cone flicker. At those levels, the flickering the 609-nm light alone produced no visible color or brightness

change. Only at much higher multiples of its threshold, and so in the midst of very strong flicker, did the appearance of the 609-nm light clearly begin to change, and then more in brightness than in hue.

3.6. Beat experiments

We have inferred the presence of high-frequency amplitude-modulated S-cone flicker in the early stages of the visual system from the visible products of its nonlinear distortion, even though we cannot directly perceive the flicker that generates the distortion products. The presence of an early high frequency S-cone flicker signal can also be inferred from its interaction with L/M-cone flicker. The combination of, for example, invisible 40-Hz S-cone flicker and visible 39.5-Hz L- or M-cone flicker produces a visible 0.5-Hz beating of the flicker, even though 40-Hz S-cone flicker is well above the S-cone CFF [14]. Subjectively, the beat is quite unlike the colored distortion product. It is seen as a slow waxing and waning of flicker, rather than as a slow change in color.

The open diamonds in Fig. 11, below, are the S-cone flicker modulation thresholds for detecting a beat with an L/M-cone stimulus, which was 0.5-Hz different in frequency and was just above flicker modulation threshold (see Section 2). At higher frequencies, the combined beat (open diamonds) and flicker (filled and open squares) sensitivity functions fall approximately twice as steeply with frequency as the distortion sensitivity functions (filled circles). The difference in slope is consistent with the idea that the distortion measurements, but not the flicker or beat measurements, avoid stages of sensitivity loss after the nonlinearity. The agreement between the slopes of the flicker and beat sensitivity curves in the ranges over which they overlap suggests that both are subject to similar sources of sensitivity loss. It may seem surprising that both the flicker and beat sensitivity curves should be subject to the same sensitivity losses. However, the S-cone beat sensitivity depends not only on the transmission of the S-cone flicker signal as far as the site at which the S-cone and L/M-cone flicker signals combine, but also on its transmission (along with the suprathreshold L/M-cone signal) in the common S- and L/M-cone pathway.

4. Discussion

We find a clear failure of the Talbot–Plateau Law for S-cone detected flicker, which is caused by distortion at a nonlinearity early in the S-cone pathway. We have used the distortion to measure separately the dynamics of the S-cone pathway before and after the nonlinear site.

4.1. The temporal properties of the S-cone pathway dissected

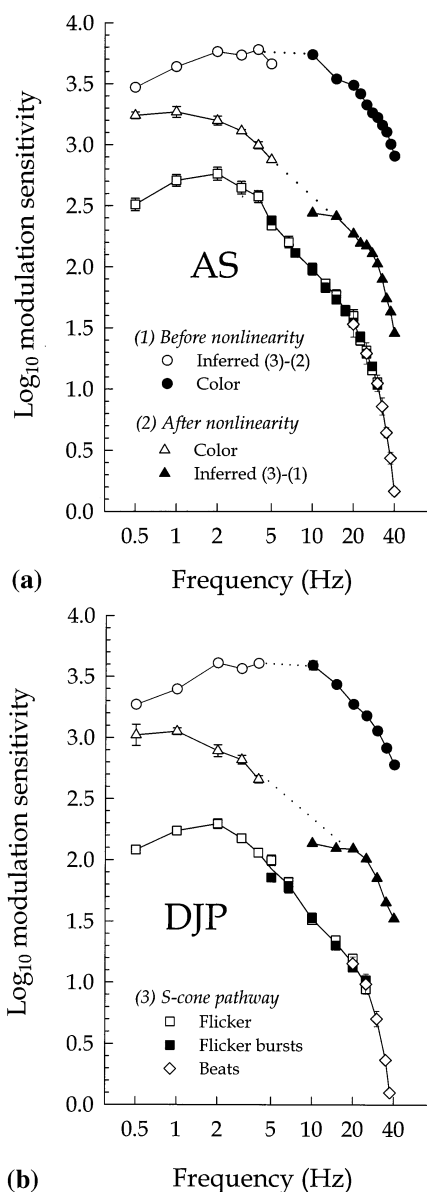


Fig. 11. Measured and inferred log_{10} S-cone temporal sensitivity functions for AS (top) and DJP (bottom) plotted against a logarithmic scale of frequency. (1) Functions assumed to apply before nonlinearity: forced-choice modulation sensitivities measured as a function of f_c (filled circles), and differences between (3) and (2) (open circles); (2) functions assumed to apply after nonlinearity: modulation sensitivities for detecting color measured as a function of f_{am} (open triangles), and differences between (3) and (1) (filled triangles); and (3) functions assumed to apply to the S-cone pathway as a whole: modulation sensitivities thresholds for detecting sinusoidal flicker (open squares), for detecting flicker bursts produced by amplitude-modulated flicker (filled squares), and for detecting beats between S-cone and L/M-cone flicker (open diamonds). The ordinate is correct for the beat sensitivity functions (open diamonds). Other functions have been vertically-shifted either to align with each other or for clarity. The dotted lines indicate the more speculative alignments.

We now combine the various modulation sensitivity functions: (1) before the nonlinearity; (2) after the nonlinearity; and (3) as a whole. If we know two of the functions, we can, in principle, infer the third from the difference between them [24]. Fig. 11 shows the functions for AS (top panel) and DJP (bottom panel). We use a log frequency scale, since it is perhaps more familiar than the linear frequency scale that we have used so far. The various functions have been shifted vertically either for clarity or to align with each other. The true vertical positions are noted in the text or can be found by referring back to the original plots of each function.

The temporal properties assumed to apply to the S-cone pathway as a whole are shown by the combination of the open diamonds, open squares and filled squares. The open diamonds are the beat sensitivities, which are correctly positioned with respect to the ordinate. The filled squares, which are the thresholds for detecting amplitude-modulated flicker as bursts of flicker (from Fig. 7, filled circles), and the open squares, which are the thresholds for continuously-presented sinusoidal flicker (from Fig. 9, open squares, with additional high frequency data), have been aligned with the open diamonds and with each other. In the regions of overlap, the three sets of data align well with one another to form the continuous function—the lowest of the three in the left and bottom panels.

The assumed temporal properties of the S-cone pathway before the nonlinearity are shown by the filled and open circles. The filled circles are the forced-choice thresholds for detecting the color change (from Fig. 7, dotted circles). The open circles are the differences between the thresholds assumed to apply after the nonlinearity (2) and those assumed to apply to the whole pathway (3).

The assumed temporal properties after the nonlinearity are shown by the filled and open triangles. The open triangles are the color thresholds modified according to the relationship between input modulation and output distortion for the nonlinearity (from Fig. 9, open circles). The filled triangles are the difference between the thresholds assumed to apply to the whole pathway (3) and those assumed to apply before the nonlinearity (1).

The vertical positions of the open circles and open triangles relative to the filled circles and filled triangles are inevitably somewhat speculative, since their frequency ranges do not overlap. One constraint, which is perhaps not obvious in the figure since the functions have been vertically separated for clarity, is that for both halves the sensitivities (1) plus (2) should equal (3). The relative positions were initially chosen so that the circles and triangles form nearly continuous func-

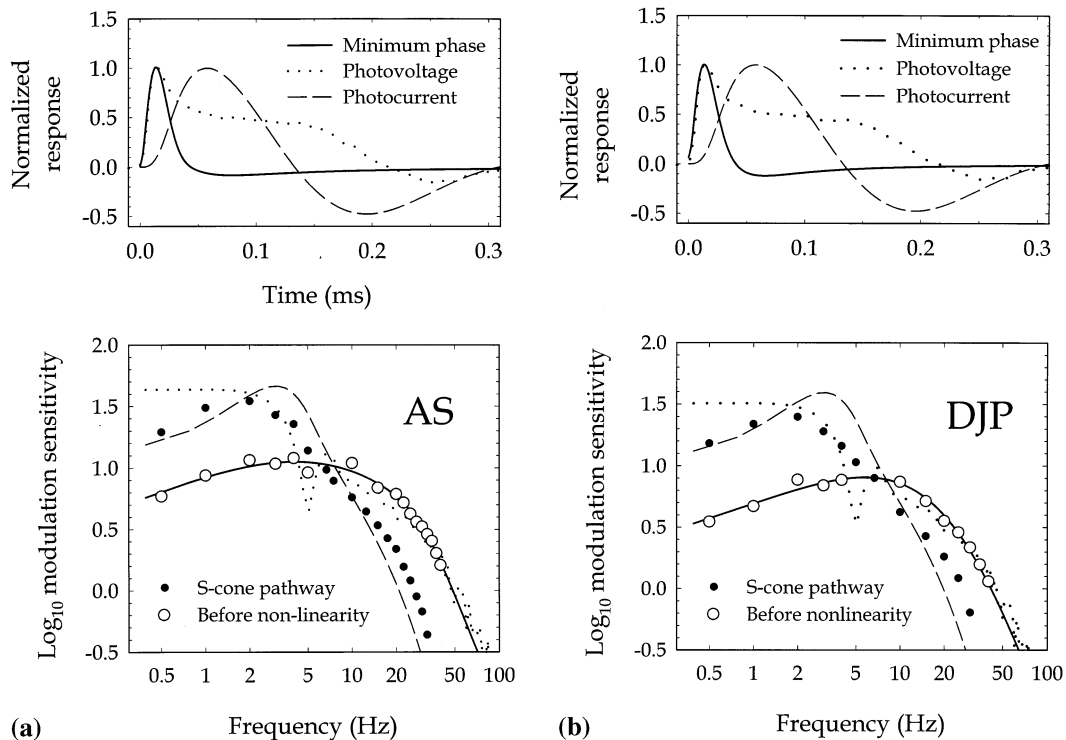


Fig. 12. Top panels: normalized photoreceptor response as a function of time. The solid line (upper left panel for AS, upper right panel for DJP) are derived by the minimum phase assumption and inverse Fourier transform from the amplitude functions assumed to apply before the nonlinearity, which are shown by the solid lines and open circles in the corresponding lower panel. The dashed lines of the upper panels show the suction electrode current recordings from a macaque S-cone photoreceptor obtained by Schnapf et al. [37] and smoothed according to their empirical formula, and with photovoltage recordings from a macaque L-cone [39]. The photovoltage trace in the both upper panels is the fastest trace of Fig. 3B in ref. [39], which was obtained at the highest flash intensity. Bottom panels: \log_{10} temporal modulation sensitivities before the nonlinearity (open circles) and the temporal modulation sensitivities for the S-cone pathway as a whole (filled circles; derived from the combined flicker, flicker burst and beat detection data shown in Fig. 11) as a function of flicker rate. The results are shown with amplitude spectra obtained from the Fourier transform of the suction electrode recordings (dashed lines), and photovoltage recordings (dotted lines) plotted in the corresponding upper panels. The solid lines fitted to the temporal modulation sensitivities (open circles) and extrapolated beyond the data are the continuous functions that were used to calculate the corresponding photoreceptor responses in the upper panels (see text for details). We note that since the pulses used to measure the photocurrent and photovoltage recordings were 10 ms in duration, the Fourier transforms shown in the lower panels are an approximation.

tions, but our final choice was also influenced by the analysis illustrated in Fig. 12.

Before the nonlinearity, the function is bandpass for both subjects, peaking between 4 and 10 Hz. The loss of sensitivity at 0.5 Hz relative to the peak is a factor of about two for both subjects. At higher frequencies, the loss of sensitivity with frequency before the nonlinearity is much shallower than for the S-cone pathway as a whole. After the nonlinearity, the function is low-pass for both subjects. There is a discontinuity for both subjects in the inferred function (filled triangles) at 15 Hz. This discontinuity may be an artifact, especially for AS, since it occurs at frequencies at which both color and flicker can be seen in the forced-choice measurements. The temporal sensitivity of the S-cone pathway as a whole is also slightly bandpass for both subjects, peaking at 2 Hz. For both subjects, the slope of the sensitivity fall-off with frequency undulates slightly, showing a minimum in slope

near 10 Hz, which may indicate the presence of two pathways.

Implicit in the above discussion is the assumption of a single S-cone pathway. An alternative possibility is that there are two pathways (see Fig. 16): one that is more sensitive at low frequencies and transmits the colored low frequency flicker and the low frequency distortion product, which can cancel each other; and a second that is more sensitive at high frequencies and transmits the achromatic flicker, which can be flicker photometrically canceled by L/M-cone flicker [26]. A dual pathway model would imply that the low-frequency portions of curves (3) and (2) in Fig. 11 apply to the pathway more sensitive at low frequencies, whereas the high frequency portions of (3) and (2) apply instead to the one more sensitive at high frequencies. Given that the nonlinearity is common to both pathways (see below), the interpretation of the curves before the nonlinearity (1) is unaffected.

4.2. The early frequency response and the photoreceptor

The shallowness of the temporal modulation sensitivity function measured before the nonlinearity suggests that the nonlinearity precedes stages that selectively reduce high frequency sensitivity. The nonlinear site is therefore likely to be relatively early in the S-cone pathway. Other evidence, such as the immunity of the distortion product to cancellation by L- or M-cone flicker, and physiological data (see Section 4.6) suggest that the nonlinearity is retinal. If the nonlinear site is only a few synapses into the visual system, then the S-cone temporal sensitivity measured before the nonlinearity may closely resemble that of the S-cone photoreceptors.

The temporal modulation sensitivities measured before the nonlinearity provide an estimate of the amplitude of the early S-cone response as a function of frequency. We would like to compare these data with photoreceptor recordings, but typically such recordings measure the photoreceptor's response to a brief pulse of light measured as a function of the time following the pulse. The photoreceptor responses are in the temporal domain, whereas our data are in the frequency domain. It is straightforward to transform data from the frequency domain to the time domain using an inverse Fourier transform, and vice versa using a Fourier transform. However, a complete characterization of the temporal properties of a system in the frequency domain requires a knowledge of the phase of the response at each frequency, as well as its amplitude.

Unfortunately, our psychophysical experiments thus far reveal no information about phase, so that we must make assumptions. We have made the usual assumption that the system before the nonlinearity is a 'minimum phase' system. Using standard formulae, we can then calculate the phase from the amplitude data (for further details see refs. [35,36]), and, finally, by an inverse Fourier transform, calculate the photoreceptor response. The estimates of the photoreceptor responses based on the minimum phase assumption are shown by the solid lines in Fig. 12 for AS (upper left panel) and DJP (upper right panel). The actual frequency responses from which they were derived are the continuous functions shown in the lower left panel for AS and lower right panel for DJP (solid lines), which are functions that were fitted to the modulation sensitivity data and extrapolated to lower and higher frequencies. The extrapolations were necessary, because, although the calculation of minimum phase at any given frequency depends mainly on the change in amplitude at that frequency, it depends also—with a weight that decreases rapidly away from the frequency of interest—on the changes in amplitude at neighboring frequencies. We needed, therefore, to predict the amplitudes outside

the range of our measurements. We assumed that the high frequency slope gradually reached and then maintained a logarithmic slope of -3 (the next highest negative integer slope for the data of both subjects) and that at low frequencies the slope was $+0.33$. The low frequency extrapolation affects mainly the late slightly negative lobe of the response, while the high frequency one affects mainly the early part of the photoreceptor response.

Initially, we compared our psychophysical results with the photocurrent response of an isolated macaque S-cone to a 10-ms flash of light [37]. The two upper panels of Fig. 12 show the S-cone photocurrent response (dashed lines), simplified according to Schnapf et al. [37]. The S-cone response as a function of frequency can be estimated from the Fourier transform of the current recording, which is shown as the dashed lines in the lower panels of Fig. 12. The functions derived from the suction electrode recordings fall much more steeply with frequency than the function measured before the nonlinearity (open circles). Indeed, the derived function is even steeper than the psychophysical function averaged from flicker and beat modulation sensitivity measurements (filled circles), which is assumed to reflect the sensitivity of the whole S-cone pathway. The differences between the psychophysical and photocurrent responses shown in the upper and lower panels of Fig. 12 question the usefulness of current recordings as a way of measuring the photoreceptor response that is transmitted to the later stages of the visual system. It might be argued that the differences between the current recordings and our measurements arise because different adaptation levels were used, but current and ERG recordings suggest that the photoreceptor response changes little with light adaptation until high intensity levels [37,38], much higher than the S-cone intensity levels used here.

Recent photovoltage recordings of macaque M- and L-cone photoreceptors are much more transient than the photocurrent recordings, having times to peak of between 10 to 35 ms [39], which are in agreement with the estimates of 13–14 ms for our subjects (see Fig. 12). For comparison, a photovoltage record from Schneeweis and Schnapf [39] is shown in each of the upper panels of Fig. 14 (dotted lines): it is the fastest of the five responses of a macaque L-cone to 10-ms flashes of 660-nm light. We chose this response because its time to peak agrees best with the response inferred from psychophysics. Yet, though the rising phase of the response, and the time to peak, agree well with the estimated responses for AS and DJP, the falling phase is much more sluggish than those suggested by psychophysics. If elements after the photoreceptor temporally sharpen the visual response by turning off more quickly than the photoreceptor, then both the photovoltage and psychophysical estimates could be correct, but for dif-

ferent stages of the visual pathway (a similar argument could be invoked to account for sluggishness of the photoreceptor current responses).

By contrasting photovoltage responses to 500 and 660-nm flashes, however, Schneeweis and Schnapf [39] showed that cone responses to 500-nm flashes are contaminated by rods. In fact, the cone responses to 660-nm flashes, such as those shown in Fig. 14, are probably also rod-contaminated¹. Consequently, the sluggish falling phase of the photovoltage responses, and the differences between the photovoltage and psychophysical estimates of the photoreceptor response shown in Fig. 12 may be due to rods. We have the advantage in our experiments that the orange background, which is 3.71 log scotopic td, is rod saturating. Thus, our measurements should reflect responses only from cones.

Chen and Makous [21] also used nonlinear distortion to measure the temporal sensitivity of the early stages of the visual system. They took advantage of a nonlinear interaction between two high-spatial-frequency laser interference gratings of the same frequency, but slightly different orientations, the distortion of which produced a low-frequency sinusoidal grating that was perpendicular to the high frequency ones. By drifting both high-frequency gratings together in a direction parallel to the low frequency one, they could temporally modulate the stages before the nonlinearity without modulating the distortion grating. They were thus able to probe the temporal sensitivity of the stages before the nonlinearity by measuring the sensitivity to the low-frequency distortion grating as a function of the drift rate of the two high frequency gratings. While it is likely that the nonlinearity probed in our experiments is different from the one probed by Chen and Makous [21], both our study and theirs found early temporal frequency responses that extend to high frequencies with a relatively shallow decline in sensitivity with increasing frequency. However, the high frequency slope that they found is only -1 in log–log coordinates, whereas the one that we found is roughly -3 . If the Chen and Makous data truly reflect the photoreceptor response, then the steeper slope found in our data must be due to stages intervening between the photoreceptor and the nonlinear site. However, unlike our data, their data are difficult to reconcile with measured photoreceptor responses.

¹ Using their estimate that 660-nm flashes must be 4574 times more radiant than the 500-nm ones to be equivalent for rods [39], we calculated that the five 660-nm flashes used to obtain the records of Fig. 3(B) are scotopically equivalent to 500-nm flashes with flash densities of between 1.79×10^0 and 1.80×10^2 log quanta μm^{-2} . Since Schneeweis and Schnapf used 500-nm flash densities of between 5×10^0 and 2.30×10^3 log quanta μm^{-2} to obtain the nine rod responses [39], we can conclude that the higher 660-nm flash densities used to stimulate cones are also potent rod stimuli.

Chen et al. [24] have reported evidence that signals from different cones interact before reaching the nonlinear stage that distorts L- and M-cone detected interference patterns. Though, as we have already argued, the nonlinear stage revealed in such experiments is unlikely to be the same as the one studied here, we must, since we have no clear evidence to the contrary, leave open the possibility that the S-cone temporal frequency response prior to the S-cone nonlinearity reflects interactions between more than one photoreceptor.

Burns and Elsner [40] took advantage of an early nonlinearity revealed in the electroretinogram (ERG) to measure the temporal frequency response of the early visual pathway electrophysiologically. The form of the frequency responses before the ERG nonlinearity [40] and before the S-cone nonlinearity (Fig. 12) are similar. Not surprisingly, however, since their measurements do not depend on visible signals, the ERG frequency response extends to higher frequencies than the psychophysical one. It also shows slightly less low-frequency sensitivity loss.

4.3. A ceiling model

Initially, we assumed that the compressive nonlinearity was a smooth or ‘soft’ function, such as a logarithmic or power function (i.e. a continuous, differentiable function). Since the most significant nonlinear term in the Taylor’s series expansions of such functions is quadratic [25], we expected that the function relating input modulation to the output distortion would be roughly quadratic. Our finding that this function was closer to linear (see Fig. 6) suggested that the nonlinearity might be a ‘hard’ one; i.e. one with an abrupt change in its input–output function, such as a full-wave rectifier [25]. One type of hard nonlinearity that produces a linear relationship between input modulation and output distortion is a saturating one that is linear at low input levels, but at high levels reaches a fixed ceiling, beyond which the output signal remains fixed at the ceiling level. Such a nonlinearity can account for many of the features of our data.

Fig. 13 shows a nonlinearity with a linear input–output function at low input levels, but a fixed output (ceiling) at high input levels. In our model, we assume that the mean S-cone level approaches and exceeds the ceiling level as the S-cone adaptation level is increased. In Fig. 13, we have simulated increases in the mean S-cone level by shifting the nonlinearity to the right. As the mean S-cone level rises, the amplitude-modulated input signal is clipped at lower and lower levels. Four instances are shown in Fig. 13: with the mean S-cone level at (1) 50, (2) 75, (3) 100 and (4) 125% of the ceiling level of 100%. Using MathCad (MathSoft, Cambridge, MA), we calculated the effect of varying the mean

S-cone level and the percentage modulation on the relative amplitudes after the nonlinearity of (1) the combined higher frequency sinusoidal components $f_c - f_{am} \oplus f_c \oplus f_c + f_{am}$ (i.e. the same components that were present in the input signal), which remain in the ratio 0.25:0.5:0.25 to produce, in the midst of other frequency components, an amplitude-modulated signal at the output; (2) the low-frequency distortion signal at f_{am} (Fig. 14, upper right); and (3) the low-frequency distortion signal at twice f_{am} (Fig. 14, bottom) (distortion signals at higher multiples of f_{am} become increasingly insignificant). The mean S-cone level is given as a percentage of the ceiling level. The output amplitudes in Fig. 14 are plotted relative to the maximum amplitude of the amplitude-modulated signal at the input. Distortion products are also produced at twice $f_c - f_{am}$, f_c and $f_c + f_{am}$, but since they are smaller than the original frequency components, and more attenuated by the late filter after the nonlinearity (see Fig. 11), they should be visually unimportant in these experiments. We assume that at mean S-cone levels of 50% or less of the ceiling level, flicker signals are unaffected by the ceiling, even at 100% modulation.

Four features of Fig. 14 are of interest. First, the low-frequency distortion (upper right panel) reaches a maximum at a mean S-cone level of 100% and falls off symmetrically at lower and higher levels. In cross-section, this triangular function resembles the rise and fall of the color CFFs for AS and DJP (see Fig. 15). In contrast, the relative amplitude of the high frequency signal falls continuously as the mean S-cone level in-

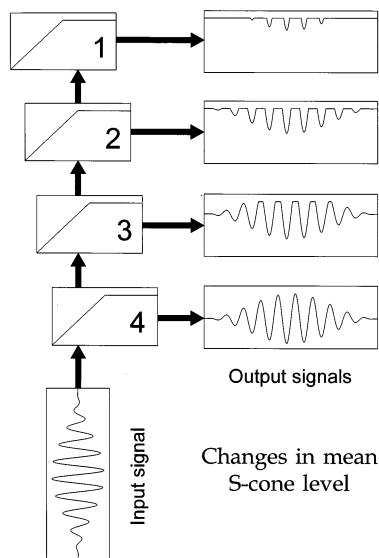


Fig. 13. The effect of passing amplitude-modulated sinusoidal flicker (input signal) with different mean levels through a nonlinearity with a linear input–output function at low inputs, but a fixed ceiling at high inputs (1–4). Changes in mean level are simulated by shifting the nonlinearity laterally: mean levels of (1) 50, (2) 75, (3) 100 and (4) 125% of the ceiling level of 100% are shown.

creases at all modulation levels (upper left panel). Second, the relative amplitudes of the high frequency signal (upper left panel) are linearly related to percentage modulation only at mean S-cone levels of 50 and 100%. At other levels, the growth is nonlinear. This behavior is discussed in the next section. Third, when the relative amplitudes of the low-frequency distortion signal (upper right panel) increase, they do so linearly with percentage modulation. However, the distortion only occurs when the modulation of the input signal (which is always assumed to be around the mean) is either: (1) large enough to reach the ceiling for mean S-cone levels $< 100\%$ (left slope) or (2) large enough to fall below the ceiling for mean S-cone levels $> 100\%$ (right slope). With the exception of the mean S-cone level of 100%, the linear increase is therefore preceded by region of zero slope. Fourth, distortion at twice f_{am} is absent at a mean S-cone level of 100% (bottom panel), but grows symmetrically at higher and lower levels before falling to zero again at 50 and 150%. In our experimental work, we did not see a clear distortion signal at twice f_{am} , which suggests, if the ceiling model is correct, that we were working mainly near a mean S-cone level of 100% (i.e. with the mean level coinciding with the ceiling). Given that the greatest distortion at f_{am} is found at the 100% level (see Fig. 14, upper right panel), and that we optimized the 440-nm radiance to maximize the distortion, we are indeed likely to have been working near that level.

The plot shown in the upper right panel of Fig. 14 can help to explain the small differences between the experimental input modulation versus output distortion functions for DJP and AS (see Fig. 6). The linear function for DJP, which passes through the origin, suggests that the mean S-cone level for him was 100%. In contrast, the best-fitting linear function for AS, which crosses that abscissa at an amplitude-modulation of 0.08 (see Fig. 6), suggests that the mean S-cone level for him was either 97 or 100% (both of which produce the same function).

If the mean S-cone level is allowed to increase with increasing S-cone adaptation, thus causing a saturation of the S-cone response as it approaches and exceeds the ceiling level, the model can also account for the color (open circles) and flicker (filled circles) CFF data, which are shown in Fig. 15 for AS (lower left panel) and for DJP (lower right panel). The upper panels of Fig. 15 plot the mean S-cone level (dashed lines) plotted as a percentage of the maximum, ceiling level (solid lines).

The flicker and color CFF predictions of the model are shown as the solid and dashed lines, respectively, in the lower panels of Fig. 15. We emphasize, however, that this model is provided mainly as a demonstration that both the flicker and the color CFFs can be accounted for by a common mechanism. The details are speculative.

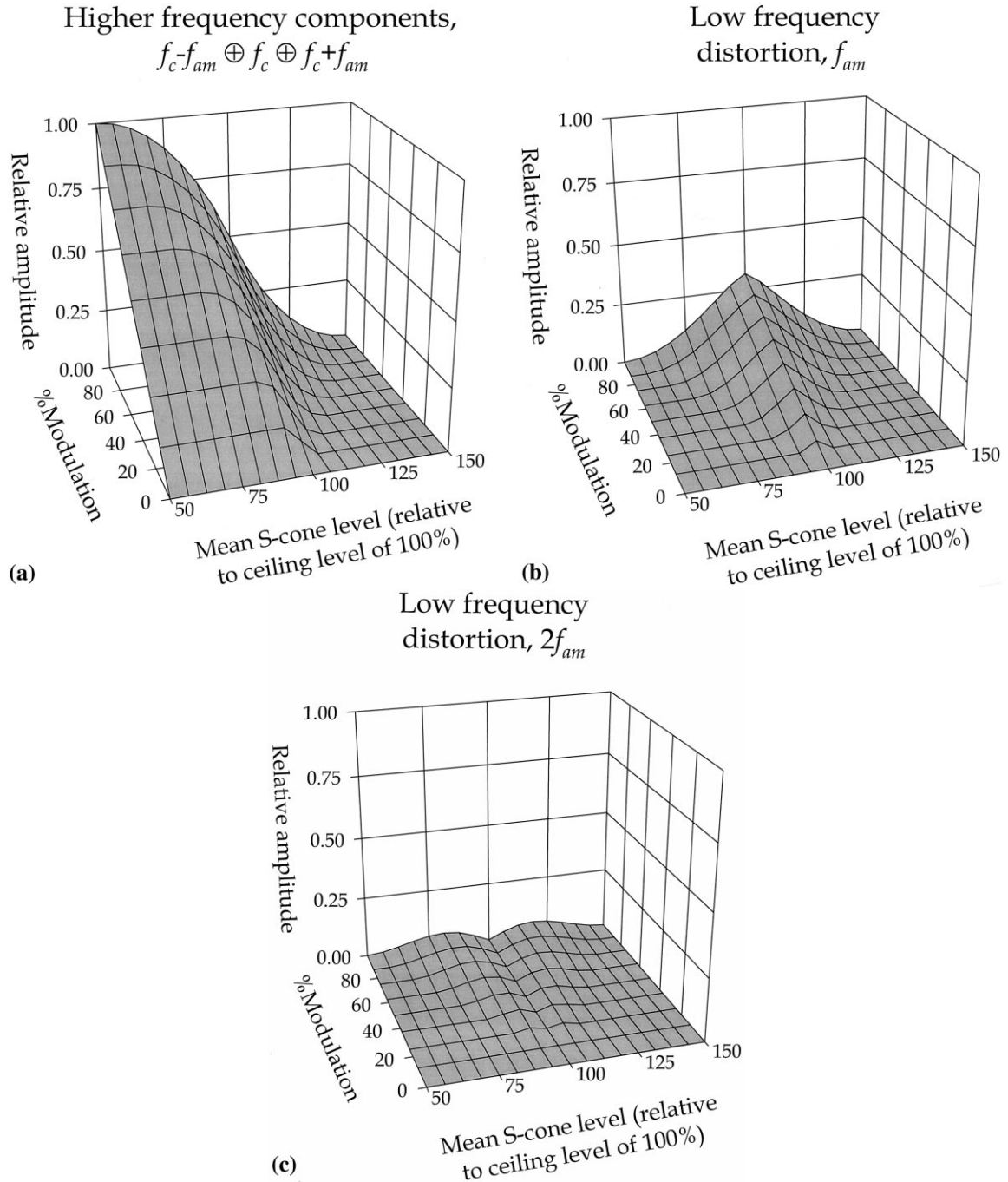


Fig. 14. 3-D plots showing the effect of varying the percentage modulation and the ceiling level on the relative output amplitudes of the combined higher frequency components of the amplitude-modulated output signal which made up of f_c , $f_c - f_{am}$ and $f_c + f_{am}$ (left panel), the distortion product at f_{am} (middle panel) and the distortion product at twice f_{am} (right panel). The amplitudes are relative to the maximum amplitude of the waveform before the nonlinearity.

The details of the model are as follows: (1) The relative amplitudes of the high-frequency carrier at f_c and the low-frequency distortion at f_{am} are assumed to vary with the mean S-cone level according to the calculated values shown in the upper panels of Fig. 14. For CFF measurements, which are carried out at maximum modulation, the relevant values are those on the rear-most planes of the graphs in Fig. 14. (The steady

intense orange background has a small direct effect on the S-cones, and thus slightly reduces the S-cone modulation as the radiance of the violet target is decreased. We ignore this small effect.) (2) For simplicity, we assume that the mean S-cone level grows linearly with log radiance, as indicated in the upper panels of both figures. The slopes and intercepts of the function relating log radiance to ceiling level were chosen so that

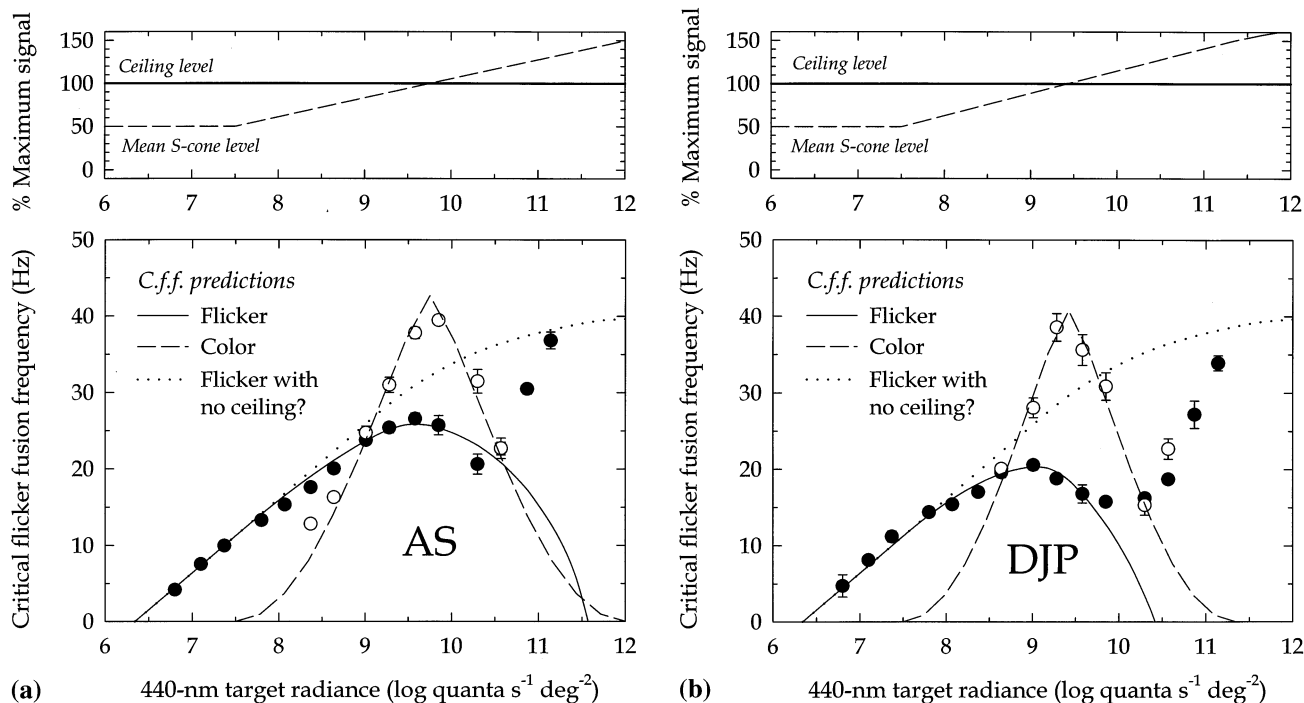


Fig. 15. Upper panels: assumed change in the mean S-cone level with target radiance (dashed lines) relative to the ceiling level (solid lines) for AS (left panel) and DJP (right panel). Lower panels: flicker (continuous lines) and color (dashed line) CFF functions as a function of \log_{10} target radiance predicted by the ceiling model compared with flicker (filled circles) and color (open circles) CFF data for AS (left panel) and DJP (right panel). The CFF functions that are assumed to apply in the absence of a ceiling (dotted lines) are the same for AS and DJP.

when scaled the low frequency distortion at f_{am} fitted the color CFF data. After $7.50 \log_{10} \text{ quanta s}^{-1} \text{ deg}^{-2}$, before which it is 50%, the mean S-cone level is assumed to rise by 22.22% (AS) or 26.04% (DJP) per \log_{10} unit. (3) To fit the model to the color CFF data, we also scaled the relative amplitudes of the low frequency distortion at f_{am} (see Fig. 14, upper right graph) by 134 for AS and by 128 for DJP to produce the functions shown by the dashed lines in the lower panels of Fig. 15. For simplicity, but also because its effects are difficult to predict, we ignored distortion at twice f_{am} (see Fig. 14, bottom panel). (4) The reduction in flicker CFF at each radiance can be estimated from the assumed reduction in the relative amplitude due to the fall in the relative ceiling level (see Fig. 14, upper left graph), and from the slope of the modulation sensitivity functions (see Fig. 3, open circles). The slopes of the latter at high frequencies are $0.04 \log_{10} \text{ units Hz}^{-1}$ for AS and $0.02 \log_{10} \text{ units Hz}^{-1}$ for DJP. We assume that the reduction in flicker CFF in Hz is the logarithmic reduction in amplitude at each radiance divided by the above slopes in log units per Hz. The reductions are the differences between the dotted lines and solid lines in the lower panels of Fig. 15. (5) We assume that the underlying flicker CFF, from which we calculated the actual flicker CFF (continuous lines, lower panels Fig. 15)—as described in (4), has the form shown by the dotted lines in the lower panels of Fig. 15. The function

is identical for both subjects. Though largely speculative, the function has a shape typical of many previously measured CFF functions [41–44]. It grows as a linear function of log radiance, in accordance with the Ferry–Porter law [30,31], with a slope of 9.7 Hz per \log_{10} unit, falling off only at high radiances. The fall-off is needed to account only for the data for AS.

This simple model provides a good account of both the flicker and the color CFF data, which suggests that both the flicker saturation and the colored distortion are produced at a single common nonlinearity. An alternative model, which is inconsistent with our data, is one in which the nonlinearity is in a pathway that is entirely separate from the one that determines flicker sensitivity. The model illustrated in Fig. 16, shows, therefore, a single nonlinearity in the S-cone pathway.

Saturation in the S-cone pathway is also found with flashed S-cone targets presented on mixed violet and yellow adapting fields [45]. The effect reported by Mollon and Polden is almost certainly the same as the saturation reported here, since it occurs under comparable short- and long-wavelength adaptation conditions. Like the saturation in the CFF, the saturation in the threshold versus increment curves of Mollon and Polden [45] are consistent with the S-cone signal reaching a ceiling as the S-cone excitation increases.

Using a nulling procedure, Kelly [25] also estimated the input modulation versus output distortion relation-

ship for the nonlinearity that produces the apparent spatial frequency doubling of gratings of low spatial frequency and high temporal frequency. He measured the modulation of a real sinusoidal grating of twice the frequency of the original stimulus that was required to null the frequency-doubled component as a function of the modulation of the original low frequency sinusoid. Instead of the expected quadratic relationship, he found a power function with an exponent of less than one. To explain his result, Kelly proposed that the underlying nonlinearity was a full-wave rectifier, followed by a compressive nonlinearity. A full-wave rectifier, like a mean S-cone level that coincides with the ceiling level (which is equivalent to an inverted half-wave rectifier), produces a linear relationship between the input modulation and the output distortion.

4.4. S-cone postreceptoral pathways

Vision mediated by the S-cones is generally assumed to be more limited than vision mediated by the other cones in both the spatial and the temporal domains. In the temporal domain, however, it has become clear that the limitations are less severe than was previously thought. Rather than having a temporal frequency response that is predominantly lowpass with a steep fall-off in sensitivity at high frequencies [46,47], the S-cone response can be bandpass with a shallow fall-off in sensitivity that is similar to the L- and M-cone responses under comparable conditions [14,26,48]. The restricted temporal properties, as well as the colored appearance of S-cone flicker, have led many researchers to conclude that the S-cone signal is confined to the sluggish visual pathways that carry chromatic information, and is excluded from the faster luminance pathways [49–55]. A defining property of the luminance

pathway is that its signals can be flicker photometrically nulled, whatever the stimulus that produces them. The demonstration that S-cones can flicker-photometrically cancel flicker signals generated by the L- or M-cones suggests that the S-cones have an input to the luminance channel [26,33].

The results presented here could be consistent with single or dual S-cone pathway. A single S-cone pathway, however, would have to generate an achromatic flicker percept at high frequencies, which can be nulled by L- or M-cone flicker, and a slow color change at low frequencies produced either by the distortion of amplitude-modulated flicker at the nonlinearity or by low frequency flicker. Such a scheme is illustrated in Fig. 16. The finding that L/M-cone flicker can null the S-cone flicker, without affecting the S-cone distortion product (see above), suggests that the cancellation of S-cone flicker by L/M-cone flicker must occur after the nonlinearity, as shown in Fig. 16. The negative sign at the site of combination reflects the inverted sign implied by the phase data of Fig. 10.

Alternatively, two S-cone pathways could bifurcate after the common nonlinearity. One pathway, which generates the achromatic percept, joins with the L- and M-cone pathways as before. The other pathway, which signals the slow color change, avoids this site. The dual channel alternative is indicated by the dashed line in the upper right corner of Fig. 16. These two channels could be entirely distinct, passing through separate nonlinearities. We know, however, from the modeling of the CFF data that the two nonlinearities have the same or similar properties. The main evidence for a duality in the present work is the subjective difference in the appearance of low and high frequency flicker. Earlier evidence comes from the masking experiments of Stockman et al. [26].

Since our flicker cancellation and distortion experiments did not extend below an f_c of 10 Hz, we have limited information about low frequency inputs from other cones (attempts to cancel low frequency S-cone flicker with L/M-cone flicker, for example, were unsuccessful, mainly because the low frequency L/M-cone flicker is itself chromatic). The connection, labeled \otimes in Fig. 16 between the M- and L-cones and the S-cones before the nonlinearity, indicates the possibility that there may be L/M-cone inputs before the nonlinearity, into a common gain control, where they may influence the relative ceiling level. Indeed, such inputs may oppose the effects of the S-cone signal at the gain control. The immunity of the distortion product to L/M-cone flicker, suggests that any gain control before the nonlinearity must be sluggish, and unable to follow frequencies > 10 Hz. The early gain control may be multiplicative, or, as suggested in a recent review article, subtractive [56].

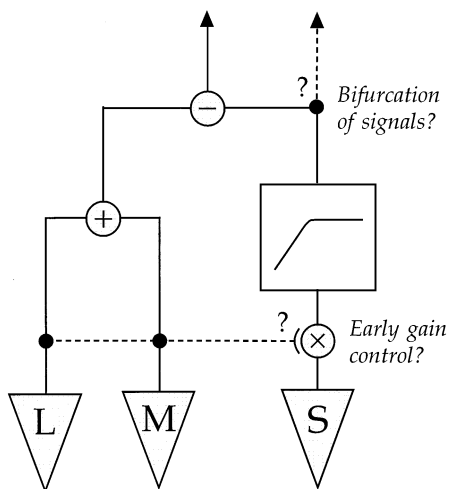


Fig. 16. Tentative model of the connections of L, M and S-cones relative to the position of the nonlinearity. The putative connections are discussed in the text.

With a spectrally-opponent gain control before the nonlinearity, the early part of the model shown in Fig. 16 is comparable to the model of Pugh and Mollon [57]. They proposed a two-site model of sensitivity control in the S-cone pathway, in which the gain at the first site is controlled by the S-cones, and the gain at the second site is controlled by the difference between S-cone and L- and M-cone signals. Thus, the S-cone pathway can become saturated when the second site is polarized either in the blue (S) direction or in the yellow (L + M) direction. Our data and model reflect saturation in the blue direction.

It is likely that varying the radiance of the orange background would, by changing the M- and L-cone excitations, alter the gain at the second site, and so alter the mean S-cone level and the target radiances at which clipping occurs. Since we did not manipulate the radiance of the orange background, which had to be kept at a high level to maintain S-cone isolation at high temporal frequencies, we have no evidence about such effects. There is, of course, ample evidence for an M- and L-cone influence on S-cone sensitivity [58,59].

4.5. Some implications of the response ceiling model

4.5.1. Effect on the shape of temporal sensitivity functions

As well as decreasing overall sensitivity, a ceiling can distort the shapes of temporal (and spatial) modulation sensitivity functions measured with sinusoidal flicker. The changes occur because, except at mean S-cone levels of 50, 100 and 150% of the ceiling level, clipping produces a nonlinear relationship between the input modulation and the relative output amplitude at the same frequency as the input signal (see Fig. 14, upper left panel). Between levels of 50 and 100%, the slopes of the input–output functions are steeper at low modulations than at high. Sensitivity functions with threshold modulations that span these changes in slope will therefore be distorted, with modulation thresholds falling above the change in slope being lowered relative to those falling below it. Given that modulation thresholds typically increase with frequency, the primary effect on temporal sensitivity curves will be to steepen the fall-off in modulation sensitivity with frequency. Between mean S-cone levels of 100 and 150%, the slope of the input–output functions is zero at low modulations. For these levels, low modulation thresholds will be lowered relative to high ones, so that the flicker sensitivity functions will be squashed or flattened.

Previous S-cone temporal modulation sensitivity measurements may show the effects of such a response ceiling. Wisowaty and Boynton [47] measured S-cone modulation sensitivities using two isolation techniques: (1) an intense yellow background to adapt selectively the M- and L-cones and (2) a target substitution that

was invisible (silent) to the M- and L-cones, but not to the S-cones. With the silent substitution method, the subjects were more sensitive overall and showed a more shallow fall-off in sensitivity at higher frequencies than with the selective adaptation method. We can explain these differences in terms of the ceiling model, if we suppose that the mean S-cone level was between 50 and 100% of the ceiling level when the yellow background was present, but was at 50% (or lower) when, in the silent substitution method, the yellow background was absent. Such an explanation requires that the intense long-wavelength background affects the ceiling level through its action on the M- and L-cones, as discussed above.

At a mean S-cone level of 100% of the ceiling level, the slope of the input–output function is linear (see Fig. 14, upper left panel). Since our measurements are likely to have been carried out at a mean S-cone level of $100 \pm 3\%$ (see above), they should be relatively unaffected by the types of distortion found at other ceiling levels.

4.5.2. Distortion at low frequencies

We have been mainly concerned with distortion produced by flicker at frequencies of 10 Hz and above. Near threshold, flicker at lower frequencies produced little visible distortion, presumably because the threshold modulation was well below the response ceiling. If the threshold is artificially raised, however, low frequency stimuli will produce visible distortion near threshold (at 0 Hz and at multiples of the stimulus frequency). Such a situation occurs in the low-frequency flicker masking experiments of Stockman et al. [26], who presented 1–10-Hz S-cone flicker in the midst of 17-Hz L/M-cone masking flicker and asked subjects to set the threshold for seeing a low-frequency color change. As confirmed in a replication of their experiment, at high modulations a steady yellow distortion product (at 0 Hz) is seen in addition to any low frequency color change that might be present. This distortion almost certainly affected the thresholds for seeing the low frequency color change, particularly since both the distortion and the color change are probably signaled by a common pathway.

4.5.3. Clipping may obscure any decline in sensitivity at low frequencies

Clipping a signal produces distortion at even harmonics of the input frequency. For a mean S-cone level of 100% of the ceiling level, for example, the amplitude of the second harmonic is $0.37 \log_{10}$ units less than the first. Threshold measurements that use moderate to high frequency flicker should be unaffected by this second harmonic, since subjects are typically much less sensitive to the second harmonic than they are to the first. If, however, the underlying temporal sensitivity is

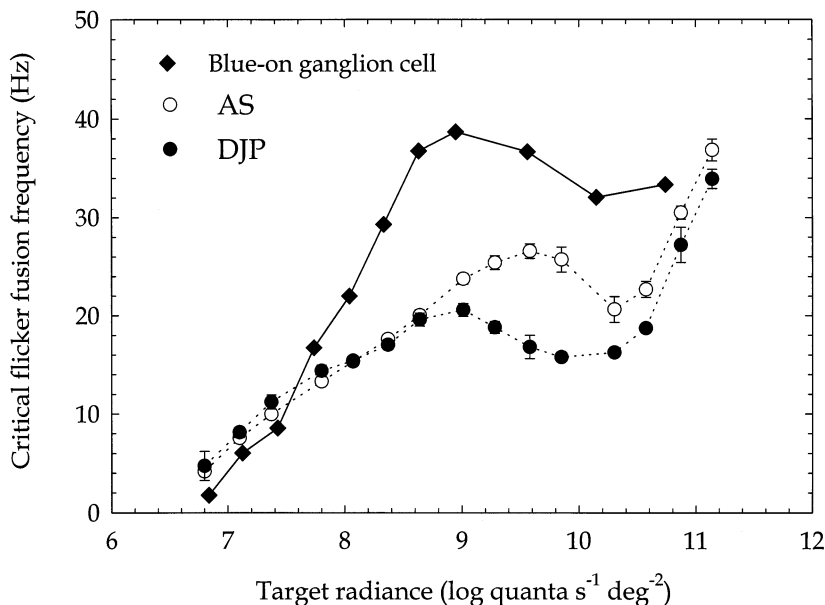


Fig. 17. Flicker CFF functions for AS (open circles) and DJP (filled circles) as a function of \log_{10} target radiance. The filled diamonds show comparable results from a single blue-on macaque ganglion cell measured by Zrenner and Gouras [60]. The human and monkey data, which were obtained with 440 and 456-nm targets, respectively, have not been corrected for differences in prereceptoral filtering or in relative cone spectral sensitivity between human and macaque. The monkey data of Zrenner and Gouras [60] were transformed from \log quanta $s^{-1} \mu m^{-2}$ to \log quanta $s^{-1} deg^{-1}$ by the assumption that $210 \mu m$ corresponds to 1° of visual angle (from the Retina Reference—see Acknowledgments).

bandpass or highpass, so that the low frequency sensitivity falls with decreasing frequency, the presence of a second harmonic may cause the low frequency fall-off to be underestimated.

4.5.4. Limited strength of the S-cone luminance input

S-cone flicker can flicker photometrically null L- and M-cone flicker only when the L/M-cone flicker is near-threshold. If the L- or M-cone flicker is raised to more than about four times threshold, the S-cone flicker signal can no longer null the L/M-cone flicker signal [26]. The limited strength of the S-cone signal can also be explained in terms of the ceiling model (see Fig. 14, upper left panel). First, at any given S-cone target radiance, the ceiling limits the maximum S-cone signal that can be produced by raising the modulation. Second, raising the radiance of the S-cone light, increases the mean S-cone signal relative to the ceiling level, and so *decreases* the S-cone signal after the nonlinearity.

4.5.5. Amplitude-modulation and side bands

As noted above, in the experiments in which f_{am} was varied from 0.5 to 5 Hz and f_c was fixed at 32.5 Hz (AS) or 25 Hz (DJP), changing f_{am} changes the frequencies of the two sidebands. As we pointed out above, since the assumed temporal frequency response before the nonlinearity is relatively shallow, changing sideband frequencies has a relatively small effect on their attenuation before the nonlinearity. Moreover, for a mean S-cone level of 100% of the ceiling level, we calculate that small increases in the amplitude of the lower

frequency sideband coupled with complementary decreases in that of the higher frequency sideband should have no effect on the size of the distortion at f_{am} . Complementary changes are expected because the \log_{10} sensitivity functions fall approximately linearly with frequency in the region of f_c (see Fig. 7).

4.6. Physiological and anatomical considerations

Fig. 17 shows an S-cone flicker CFF curve measured by Zrenner and Gouras [60] in a macaque blue-on retinal ganglion cell (diamonds), which appears remarkably similar in form to the flicker CFF curves for AS (open circles) and DJP (filled circles). The monkey data were obtained under comparable conditions to the human data (with a 456 nm target presented on an intense orange background). Although the monkey CFF data reach higher frequencies (~ 39 Hz), the overall shape of the monkey ganglion cell and human CFF data are strikingly similar: both rise steadily with \log target radiance to reach a plateau, before falling at higher radiances. Even the higher CFF for the cell is not surprising, since we know from the beat and distortion experiments (see above) that the early human S-cone pathway can detect frequencies as high as 40 Hz. This similarity between the human data and monkey ganglion cell data provides compelling evidence that the nonlinearity is at or before the ganglion cells, and therefore retinal.

Twenty-one of the 22 blue-on ganglion cells measured by Zrenner and Gouras had coextensive S-cone

ON fields in opposition to L- and M-cone OFF fields. These cells have since been identified anatomically as the small, bistratified blue-on ganglion cell type by Dacey and Lee [61]. They give sustained on-responses to S-cone stimulation, and clear off-responses to stimulation by long-wavelength lights [60,61]. The pathway from the S-cones to the blue ON bipolar cells [62,63] to the bistratified blue ON ganglion cell may be the primary S-cone pathway. Indeed, the S-cones in the central retina of the macaque may be invaginated exclusively by blue ON bipolar cells [64].

The bistratified blue ON ganglion cell fulfills the requirement that the nonlinearity must precede the combination of S-cone and L/M-cone flicker, since there is already evidence of the effects of a response ceiling in the CFF data for the cell (see Fig. 17). Moreover, as in the cell, the S-cone and L/M-cone flicker signals are opposed under the conditions of our experiment (see Fig. 11, right panel and ref. [26]). Thus, the bistratified blue ON ganglion cell might be a candidate for the retinal site at which the S-cone and L- and M-cone signals cancel each other (see Fig. 16). There are two objections to this simple correspondence, however. First, the relatively weak and sluggish S-cone flicker signal that nulls the L- and M-cone flicker signals seems more likely to be an OFF signal (and the L/M-cone signals ON) than an ON signal, since it is inverted in sign (see Fig. 11, right panel). Second, for the blue ON ganglion cell to be the site of flicker cancellation, the L- and M-cone flicker signals must be exclusively transmitted through the blue ON ganglion cells under the conditions of our experiment, since signals transmitted through other ganglion cells would remain uncanceled.

Another objection to the bistratified blue ON ganglion cell being the site of flicker cancellation is that the S-cone flicker signal under these conditions behaves in several respects like a luminance signal (see above). The contribution to flicker photometry, for instance, is not generally thought to be a property of signals in parvocellular chromatic pathways, though there is little direct evidence to support this view. Recent evidence, however, suggests that the blue ON ganglion cells actually project to the intralaminar layers of the LGN, rather than to the parvocellular layers [65].

Perhaps the blue ON ganglion cell forms part of the S-cone pathway that signals color (and is more sensitive at low frequencies), while other cells provide a separate pathway for achromatic flicker (see Fig. 16). There are other pathways available to the S-cone signals, which contact not only the invaginating blue-cone bipolar cell, but also other bipolar cells [63]. In addition to the bistratified blue ON ganglion, there is some evidence for blue OFF ganglion cells in rhesus [66] and macaque [67] monkeys. Moreover, by way of H2 and perhaps H1 horizontal cells (see below), and by way of gap junc-

tions [68] (but see [69]) S-cone signals may have access to most other postreceptoral channels. While these secondary S-cone pathways may be relatively insignificant under normal conditions of adaptation, they may be favored by the intense chromatic adaptation used in our experiments.

Since evidence for the nonlinearity is found in ganglion cell responses, it may arise in the outerplexiform layer, where H1 and H2 horizontal cells both contact M- and L-cone pedicles, but mainly the H2 cells contact S-cone pedicles [70]. In a recent study in which S-cones were labeled with an S-cone photopigment antiserum, 15% of H1 cells were found to contact S-cones, whereas all H2 cells contacted S-cones [71]. Physiologically, however, an S-cone response was found only in H2 cells [72]. If cone photoreceptors light adapt very little [37,38], then it seems likely that one function of the horizontal cell must be to control the gain of the signals transmitted from the cones to cone bipolar cells, and so maintain the responses of the bipolar cells in a useful part of their operating range. The H2 cells may be the primary gain control for the S-cone pathway. The intense orange background, which is used in our experiments to isolate the S-cone response, might saturate the H2 cells (through their M- and L-cone inputs), so that they can no longer compensate for changes in S-cone excitation. Increasing the violet target radiance on the orange background might then cause signals in the S-cone pathway to rapidly reach the response ceiling.

Acknowledgements

We are grateful to Sabine Apitz, Steve Burns, Rhea Eskew, Bruce Henning, and Walt Makous for comments on this manuscript, and Donald MacLeod for helpful discussions during the early part of this work. The Retina Reference of Lance Hahn (<http://retina.anatomy.upenn.edu/~lance/retina/retina.html>) and the Webvision page of Helga Kolb and Patricia Goede (<http://insight.med.utah.edu/Webvision>) were valuable sources of information on physiology and anatomy. This work was supported by grants NIH EY10206 and NSF IBN 92-10046.

References

- [1] Brewster D. On the influence of succession of light upon the retina. *Philos Mag* 1838;4:241.
- [2] Brücke E. Über die Nutzeffect intermitterender Netzhautreizungen. *Sitzungsberichte der Mathematisch-Naturwissenschaftlichen Classe der Kaiserlichen Akademie der Wissenschaften* 1848;49:128–153.
- [3] Bartley SH. A central mechanism in brightness enhancement. *Proc Soc Exp Biol Med* 1938;38:535–6.

- [4] Bartley SH. Some effects of intermittent photic stimulation. *J Exp Psychol* 1939;25:462–80.
- [5] Bartley SH. Brightness comparisons when one eye is stimulated intermittently and the other steadily. *J Psychol* 1951;34:165–7.
- [6] Bartley SH. Brightness enhancement in relation to target intensity. *J Psychol* 1951;32:57–62.
- [7] Stewart GN. Is the law of Talbot true for very rapidly intermittent light? *Proc R Soc Edinb* 1887;15:441–64.
- [8] Bartley SH, Nelson TM. Certain chromatic and brightness changes associated with rate of intermittency of photic stimulation. *J Psychol* 1960;50:323–32.
- [9] Ball RJ. An investigation of chromatic brightness enhancement tendencies. *Am J Optom Physiol Opt* 1964;41:333–61.
- [10] Ball RJ, Bartley SH. Changes in brightness index, saturation and hue produced by luminance–wavelength–temporal interactions. *J Opt Soc Am* 1966;66:695–9.
- [11] Talbot HF. Experiments on light. *Philos Mag Ser 3* 1834;5:321–34.
- [12] Plateau J. Sur un principe de photométrie. *Bulletins de l'Académie Royale des Sciences et Belles-lettres de Bruxelles* 1835;2:52–59.
- [13] Brindley GS. Beats produced by simultaneous stimulation of the human eye with intermittent light and intermittent or alternating electric current. *J Physiol (Lond)* 1962;164:157–67.
- [14] Stockman A, MacLeod DIA, Lebrun S. Faster than the eye can see: blue cones respond to rapid flicker. *J Opt Soc Am A* 1993;10:1396–402.
- [15] Spekrijse H, Reits D. Sequential analysis of the visual evoked potential system in man; nonlinear analysis of a sandwich system. *Ann NY Acad Sci* 1982;388:72–97.
- [16] Burton GJ. Evidence for non-linear response processes in the human visual system from measurements on the thresholds of spatial beat frequencies. *Vis Res* 1973;13:1211–25.
- [17] Victor J, Shapley R, Knight BW. Nonlinear analysis of retinal ganglion cells in the frequency domain. *Proc Natl Acad Sci USA* 1977;74:3068–72.
- [18] Marmarelis PZ, Marmarelis VZ. *Analysis of Physiological Systems: The White-Noise Approach*. New York: Plenum Press, 1978.
- [19] Trimble J, Phillips G. Nonlinear analysis of the human visual evoked response. *Biol Cybernet* 1978;30:55–61.
- [20] Victor J, Shapley R. A method of nonlinear analysis in the frequency domain. *Biophys J* 1980;29:458–83.
- [21] Chen B, Makous W. Temporal modulation at high spatial frequencies. *Invest Ophthalmol Vis Sci (Suppl)* 1990;31:428.
- [22] Burns SA, Elsner AE, Kretz MR. Analysis of nonlinearities in the flicker ERG. *Optom Vis Sci* 1992;69:95–105.
- [23] MacLeod DIA, Williams DR, Makous W. A visual nonlinearity fed by single cones. *Vis Res* 1992;32:347–63.
- [24] Chen B, Makous W, Williams DR. Serial spatial filters in vision. *Vis Res* 1993;33:413–27.
- [25] Kelly DH. Nonlinear visual responses to flickering sinusoidal grating. *J Opt Soc Am* 1981;71:1051–5.
- [26] Stockman A, MacLeod DIA, DePriest DD. The temporal properties of the human short-wave photoreceptors and their associated pathways. *Vis Res* 1991;31:189–208.
- [27] Grünbaum OFF. On intermittent stimulation of the retina. Part II. *J Physiol (Lond)* 1898;22:433–50.
- [28] Stockman A. Changes in color produced by amplitude-modulated M- and L-cone detected flickering lights survive flicker photometric cancellation. *Invest Ophthalmol Vis Sci (Suppl)* 1993;34:912.
- [29] Marks LE. Blue-sensitive cones can mediate brightness. *Vis Res* 1974;14:1493–4.
- [30] Ferry J. Persistence of vision. *Am J Sci Arts* 1892;44:192–207.
- [31] Porter TC. Contributions to the study of flicker. II. *Proc R Soc Lond* 1902;A70:313–9.
- [32] Baylor DA, Nunn BJ, Schnapf JL. Spectral sensitivity of the cones of the monkey *Macaca fascicularis*. *J Physiol (Lond)* 1987;390:145–60.
- [33] Stockman A, MacLeod DIA. An inverted S-cone input to the luminance channel: evidence for two processes in S-cone flicker detection. *Invest Ophthalmol Vis Sci (Suppl)* 1987;28:92.
- [34] Lee J, Stromeyer CF. Contribution of human short-wave cones to luminance and motion detection. *J Physiol (Lond)* 1989;413:563–93.
- [35] Bode HW. *Network Analysis and Feedback Amplifier Design*. Princeton: van Nostrand, 1945.
- [36] Murphy GJ. *Control Engineering*. Princeton: van Nostrand, 1959.
- [37] Schnapf JL, Nunn BJ, Meister M, Baylor DA. Visual transduction in cones of the monkey *Macaca fascicularis*. *J Physiol (Lond)* 1990;427:681–713.
- [38] Hood DC, Birch DG. Human cone receptor activity: The leading edge of the a-wave and models of receptor activity. *Vis Neurosci* 1993;10:857–71.
- [39] Schneeweis DM, Schnapf JL. Photovoltage of rods and cones in macaque retina. *Science* 1995;268:1053–6.
- [40] Burns SA, Elsner AE. Response of the retina at low temporal frequencies. *J Opt Soc Am A* 1996;13:667–72.
- [41] Ives HE. Studies in the photometry of lights of different colours. II. Spectral luminosity curves by the method of critical frequency. *Philos Mag Ser 6* 1912;24:352–70.
- [42] Hecht S, Verrijp CD. The influence of intensity, color and retinal location on the fusion frequency of intermittent illumination. *Proc Natl Acad Sci USA* 1933;19:522–35.
- [43] Hecht S, Smith EL. Intermittent stimulation by light. VI. Area and the relation between critical frequency and intensity. *J Gen Physiol* 1936;19:979–89.
- [44] Kelly DH. Visual responses to time-dependent stimuli I. Amplitude sensitivity measurements. *J Opt Soc Am* 1961;51:422–9.
- [45] Mollon JD, Polden PG. Saturation of a retinal cone mechanism. *Nature* 1977;259:243–6.
- [46] Kelly DH. Spatio-temporal frequency characteristics of color-vision mechanisms. *J Opt Soc Am* 1974;64:983–90.
- [47] Wisowaty JJ, Boynton RM. Temporal modulation sensitivity of the blue mechanism: measurements made without chromatic adaptation. *Vis Res* 1980;20:895–909.
- [48] Green DG. Sinusoidal flicker characteristics of the colour-sensitive mechanisms of the eye. *Vis Res* 1969;9:591–601.
- [49] Schrödinger E. Über das Verhältnis der Vierfarben zur Dreifarben-theorie. *Sitzungsberichte. Abt. 2a, Mathematik, Astronomie, Physik, Meteorologie und Mechanik. Akademie der Wissenschaften in Wien, Mathematisch-Naturwissenschaftliche Klasse* 1925;134:471.
- [50] Luther R. Aus dem Gebiet der Farbreizmetrik. *Zeitschrift für technische Physik* 1927;8:540–58.
- [51] Walls GL. A branched-pathway schema for the color-vision system and some of the evidence for it. *Am J Ophthalmol* 1955;39:8–23.
- [52] De Lange H. Research into the dynamic nature of the human fovea–cortex systems with intermittent and modulated light. II. Phase shift in brightness and delay in color perception. *J Opt Soc Am* 1958;48:784–9.
- [53] Guth SL, Alexander JV, Chumbly JI, Gillman CB, Patterson MM. Factors affecting luminance additivity at threshold. *Vis Res* 1968;8:913–28.
- [54] Smith VC, Pokorny J. Spectral sensitivity of the foveal cone photopigments between 400 and 500 nm. *Vis Res* 1975;15:161–71.
- [55] Eisner A, MacLeod DIA. Blue sensitive cones do not contribute to luminance. *J Opt Soc Am* 1980;70:121–3.
- [56] Makous WL. Fourier models and the loci of adaptation. *J Opt Soc Am A* 1997;14:2323–45.

- [57] Pugh EN, Mollon JD. A theory of the p1 and p3 color mechanisms of Stiles. *Vis Res* 1979;20:779–88.
- [58] Mollon JD. Color vision. *Annu Rev Psychol* 1982;33:41–85.
- [59] Yeh T, Smith VC, Pokorny J. Chromatic discrimination with variation in chromaticity and luminance: data and theory. *Vis Res* 1993;33:1835–45.
- [60] Zrenner E, Gouras P. Characteristics of the blue sensitive cone mechanism in primate retinal ganglion cells. *Vis Res* 1981; 21:1605–9.
- [61] Dacey DM, Lee BB. The ‘blue-on’ opponent pathway in primate retina originates from a distinct bistratified ganglion cell type. *Nature* 1994;367:731–5.
- [62] Mariani AP. Bipolar cells in monkey retina selective for the cones likely to be blue-sensitive. *Nature* 1984;308:184–6.
- [63] Kouyama N, Mashak DW. Bipolar cells specific for blue cones in the macaque retina. *J Neurosci* 1992;12:1233–52.
- [64] Herr SS, Tiv N, Sterling P, Schein SJ. S cones in macaque fovea are invaginated by one type of on bipolar cell, but L and M cones are invaginated by midget and diffuse bipolar cells. *Invest Ophthalmol Vis Sci (Suppl)* 1996;37:S1059.
- [65] Martin PR, White AJ, Goodchild AK, Wilder HD, Sefton AE. Evidence that blue-on cells are part of the third geniculocortical pathway in primates. *Eur J Neurosci* 1997;9:1536–41.
- [66] De Monasterio FM, Gouras P. Functional properties of ganglion cells of the rhesus monkey retina. *J Physiol (Lond)* 1975;251:167–95.
- [67] Valberg A, Lee BB, Tigwell DA. Neurones with strong inhibitory S-cone inputs in the macaque lateral geniculate nucleus. *Vis Res* 1986;26:1061–4.
- [68] Tsukamoto T, Masarachia P, Schein SJ, Sterling P. Gap junctions between the pedicles of macaque foveal cones. *Vis Res* 1992;10:1809–15.
- [69] Kolb H, Goede P, Roberts S, McDermott R, Gouras P. The uniqueness of the S-cone pedicle in the human retina and consequences for color processing. *J Comp Neurol* 1997;386: 443–60.
- [70] Anhalt P, Kolb H. Horizontal cells and cone photoreceptors in primate retina: a Golgi-light microscope study of spectral connectivity. *J Comp Neurol* 1994;343:387–405.
- [71] Goodchild AK, Chan TL, Grünert U. Horizontal cell connections with short-wavelength-sensitive cones in macaque monkey retina. *Vis Neurosci* 1996;13:833–45.
- [72] Dacey DM, Lee BB, Stafford DK, Pokorny J, Smith VC. Horizontal cells of the primate retina: cone specificity without spectral opponency. *Science* 1996;271:656–9.
- [73] Stockman A, MacLeod DIA, Johnson NE. Spectral sensitivities of the human cones. *J Opt Soc Am A* 1993;10:2491–521.
- [74] Stockman A, Sharpe LT, Fach CC. The spectral sensitivity of the human short-wavelength cones. *Vis Res*, in press.
- [75] Stockman A, Macleod DIA. A change in color produced by an invisibly flickering light: a comprehensive non-linearity in the S-cone pathway. *Invest Ophthalmol Vis Sci (Suppl)* 1992;33:756.
- [76] Drum B. Flicker and suprathreshold spatial summation: Evidence for a two-channel model of achromatic brightness. *Percept Psychophys* 1984;36:245–50.